13. Shattil, S. J., and Newman, P. J. (2004) *Blood* **104,** 1606–1615
14. Emambokus, N. R., and Frampton, J. (2003) *Immunity* **19,** 33–45
15. Eto, K., Murphy, R., Kerrigan, S. W., Bertoni, A., Stuhlmann, H., Nakano, T., Leavitt, A. D., and Shattil, S. J. (2002) *Proc. Natl. Acad. Sci. U.S.A.* **99,** 12819–12824
16. Kieffer, N., Fitzgerald, L. A., Wolf, D., Cheresh, D. A., and Phillips, D. R. (1991) *J. Cell Biol.* **113,** 451–461
17. Suehiro, K., Smith, J. W., and Plow, E. F. (1996) *J. Biol. Chem.* **271,** 10365–10371
18. Berlanga, O., Emambokus, N., and Frampton, J. (2005) *Exp. Hematol.* **33,** 403–412
19. Mosesson, M. W. (2005) *J. Thromb. Haemost.* **3,** 1894–1904
20. Tang, L., Jennings, T. A., and Eaton, J. W. (1998) *Proc. Natl. Acad. Sci. U.S.A.* **95,** 8841–8846
21. Drew, A. F., Liu, H., Davidson, J. M., Daugherty, C. C., and Degen, J. L. (2001) *Blood* **97,** 3691–3698
22. Szaba, F. M., and Smiley, S. T. (2002) *Blood* **99,** 1053–1059
23. Fitzgerald, J. R., Foster, T. J., and Cox, D. (2006) *Nat. Rev. Microbiol.* **4,** 445–457
24. Loughman, A., Fitzgerald, J. R., Brennan, M. P., Higgins, J., Downer, R., Cox, D., and Foster, T. J. (2005) *Mol. Microbiol.* **57,** 804–818
25. Fitzgerald, J. R., Loughman, A., Keane, F., Brennan, M., Knobel, M., Higgins, J., Visai, L., Speziale, P., Cox, D., and Foster, T. J. (2006) *Mol. Microbiol.* **59,** 212–230
26. Lengweiler, S., Smyth, S. S., Jirouskova, M., Scudder, L. E., Park, H., Moran, T., and Coller, B. S. (1999) *Biochem. Biophys. Res. Commun.* **262,** 167–173
27. Gerber, D. J., Pereira, P., Huang, S. Y., Pelletier, C., and Tonegawa, S. (1996) *Proc. Natl. Acad. Sci. U.S.A.* **93,** 14698–14703
28. Kitaura, J., Song, J., Tsai, M., Asai, K., Maeda-Yamamoto, M., Mocsai, A., Kawakami, Y., Liu, F. T., Lowell, C. A., Barisas, B. G., Galli, S. J., and Kawakami, T. (2003) *Proc. Natl. Acad. Sci. U.S.A.* **100,** 12911–12916
29. Morita, S., Kojima, T., and Kitamura, T. (2000) *Gene Ther.* **7,** 1063–1066
30. Kitamura, T., Koshino, Y., Shibata, F., Oki, T., Nakajima, H., Nosaka, T., and Kumagai, H. (2003) *Exp. Hematol.* **31,** 1007–1014
31. Furumoto, Y., Nunomura, S., Terada, T., Rivera, J., and Ra, C. (2004) *J. Biol. Chem.* **279,** 49177–49187
32. Hata, D., Kawakami, Y., Inagaki, N., Lantz, C. S., Kitamura, T., Khan, W. N., Maeda-Yamamoto, M., Miura, T., Han, W., Hartman, S. E., Yao, L., Nagai, H., Goldfeld, A. E., Alt, F. W., Galli, S. J., Witte, O. N., and Kawakami, T. (1998) *J. Exp. Med.* **187,** 1235–1247
33. Inagaki, N., Goto, S., Nagai, H., and Koda, A. (1986) *Int. Arch. Allergy Appl. Immunol.* **81,** 58–62
34. Nagai, H., Sakurai, T., Inagaki, N., and Mori, H. (1995) *Biol. Pharm. Bull.* **18,** 239–245
35. Wong, M. X., Roberts, D., Bartley, P. A., and Jackson, D. E. (2002) *J. Immunol.* **168,** 6455–6462
36. Artis, D., Humphreys, N. E., Potten, C. S., Wagner, N., Müller, W., McDermott, J. R., Grencis, R. K., and Else, K. J. (2000) *Eur. J. Immunol.* **30,** 1656–1664
37. Honda, S., Tomiyama, Y., Shiraga, M., Tadokoro, S., Takamatsu, J., Saito, H., Kurata, Y., and Matsuzawa, Y. (1998) *J. Clin. Invest.* **102,** 1183–1192
38. Flick, M. J., LaJeunesse, C. M., Talmage, K. E., Witte, D. P., Palumbo, J. S., Pinkerton, M. D., Thornton, S., and Degen, J. L. (2007) *J. Clin. Invest.* **117,** 3224–3235
39. Flick, M. J., Du, X., Witte, D. P., Jirousková, M., Soloviev, D. A., Busuttil, S. J., Plow, E. F., and Degen, J. L. (2004) *J. Clin. Invest.* **113,** 1596–1606

STEM CELLS®

TRANSLATIONAL AND CLINICAL RESEARCH

Lnk Deletion Reinforces the Function of Bone Marrow Progenitors in Promoting Neovascularization and Astrogliosis Following Spinal Cord Injury

NAOSUKE KAMEI,[a,b,c] SANG-MO KWON,[g] CANTAS ALEV,[a,d] MASAKAZU ISHIKAWA,[b] AYUMI YOKOYAMA,[a] KAZUYOSHI NAKANISHI,[b] KIYOTAKA YAMADA,[b] MIKI HORII,[a,c] HIROMI NISHIMURA,[a] SATOSHI TAKAKI,[f] ATSUHIKO KAWAMOTO,[a] MASAAKI II,[a,c] HIROSHI AKIMARU,[a,c] NOBUHIRO TANAKA,[b] SHIN-ICHI NISHIKAWA,[c] MITSUO OCHI,[b] TAKAYUKI ASAHARA[a,c,e]

[a]Group of Vascular Regeneration, Institute of Biomedical Research and Innovation, 2-2 Minatojima-minamimachi, Chuo-ku, Kobe, Hyogo 650-0047, Japan; [b]Department of Orthopaedic Surgery, Graduate School of Biomedical Sciences, Hiroshima University, 1-2-3 Kasumi, Minami-ku, Hiroshima City, Hiroshima 734-8551, Japan; [c]Laboratory for Stem Cell Biology; [d]Laboratory for Early Embryogenesis, RIKEN Center for Developmental Biology, 2-2-3 Minatojima-minamimachi, Chuo-ku, Kobe, Hyogo 650-0047, Japan; [e]Department of Regenerative Medicine, Tokai University School of Medicine, 143 Shimokasuya, Isehara-shi, Kanagawa 259-1193, Japan; [f]Department of Community Health and Medicine, Research Institute, International Medical Center of Japan, 1-21-1 Toyama, Shinjuku-ku, Tokyo 162-8655, Japan; [g]Department of Biomedical Science, Laboratory for Vascular Medicine & Stem Cell Biology, CHA University, Seoul, Korea

Key Words. Lnk • Bone marrow • Angiogenesis • Astrogliogenesis • Spinal cord injury • Regeneration

ABSTRACT

Lnk is an intracellular adaptor protein reported as a negative regulator of proliferation in c-Kit positive, Sca-1 positive, lineage marker-negative (KSL) bone marrow cells. The KSL fraction in mouse bone marrow is believed to represent a population of hematopoietic and endothelial progenitor cells (EPCs). We report here that, in vitro, $Lnk^{-/-}$ KSL cells form more EPC colonies than $Lnk^{+/+}$ KSL cells and show higher expression levels of endothelial marker genes, including CD105, CD144, Tie-1, and Tie2, than their wild-type counterparts. In vivo, the administration of $Lnk^{+/+}$ KSL cells to a mouse spinal cord injury model promoted angiogenesis, astrogliosis, axon growth, and functional recovery following injury, with $Lnk^{-/-}$ KSL being significantly more effective in inducing and promoting these regenerative events. At day 3 following injury, large vessels could be observed in spinal cords treated with KSL cells, and reactive astrocytes were found to have migrated along these large vessels. We could further show that the enhancement of astrogliosis appears to be caused in conjunction with the acceleration of angiogenesis. These findings suggest that Lnk deletion reinforces the commitment of KSL cells to EPCs, promoting subsequent repair of injured spinal cord through the acceleration of angiogenesis and astrogliosis. STEM CELLS *2010;28:365–375*

Disclosure of potential conflicts of interest is found at the end of this article.

INTRODUCTION

The population of c-Kit-positive, Sca-1-positive, lineage marker-negative (KSL) cells in mouse bone marrow is well known to represent a fraction of hematopoietic stem/progenitor cells (HSCs) [1]. The KSL cell population is also believed to be a good source for endothelial progenitor cells (EPCs), with a portion of KSL cells able to differentiate into the endothelial lineage and to contribute to vasculogenesis in vivo [2–4]. Previous studies reported that the transplantation of human circulating CD34 positive cells believed to contain HSCs and EPCs was effective in enhancing repair and regeneration of the central nervous system (CNS) [5–7]. Other previous studies have shown that functional recovery of hindlimbs in mouse spinal cord injury (SCI) models was improved by the transplantation of mouse bone marrow KSL cells [8, 9]. However, the mechanisms for spinal cord repair promoted by KSL cell transplantation remain to be clarified.

Author contributions: N.K.: conception and design, collection and/or assembly of data, data analysis and interpretation, manuscript writing; S.M.K.: conception and design, collection and/or assembly of data; N.K. and S.M.K.: contributed equally to this work; C.A.: collection and/or assembly of data, manuscript writing; M.I., A.Y., K.N., K.Y., M.H., and M.I.: collection and/or assembly of data; H.N., S.T., and H.A.: conception and design; A.K.: manuscript writing; N.T., S.N., and M.O.: administrative support; T.A.: conception and design, administrative support.

Correspondence: Takayuki Asahara, M.D., Ph.D., Group of Vascular Regeneration, Institute of Biomedical Research and Innovation, 2-2 Minatojima-minamimachi, Chuo-ku, Kobe, Hyogo 650-0047, Japan. Telephone: +81-78-304-5772; Fax: +81-78-304-5772; e-mail: asa777@is.icc.u-tokai.ac.jp Received August 20, 2009; accepted for publication October 16, 2009; first published online in STEM CELLS *EXPRESS* January 28, 2010. 1066-5099/2009/$30.00/0 doi: 10.1002/stem.243

Lnk is an adaptor protein expressed in KSL cells and believed to negatively regulate the key signaling pathways for the proliferation of KSL cells such as stem cell factor (SCF) signaling and thrombopoietin signaling [10–12]. In Lnk-deficient mice, the proliferation of KSL cells is upregulated and the number of KSL cells in bone marrow is increased compared to that in wild-type mice [10]. We hypothesized that the transplantation of Lnk-deficient KSL cells might be more effective in promoting repair of injured spinal cord than wild-type KSL cells. The purpose of this study was to assess the effect of Lnk-deficient KSL cell transplantation on the regeneration of injured spinal cord and to clarify the mechanisms of spinal cord repair promoted by the transplantation of KSL cells.

Materials and Methods

The Institutional Animal Care and Use Committees of RIKEN Center for Developmental Biology approved all animal procedures in this study.

Generation of Lnk-Deficient Mice

Lnk knockout mice were generated as reported previously [10, 13]. The mice used in this study were backcrossed with C57BL/6 > 10 times. They were bred and maintained at the animal facility of RIKEN Center for Developmental Biology (Kobe, Japan, http://www.cdb.riken.jp/en/index.html).

Isolation of KSL Cells

KSL cells were purified from bone marrow cells by a modification of the method reported previously [14]. Bone marrow cells were obtained from C57BL/6 mice (wild-type mice) or Lnk knockout mice. Lineage-positive cells were removed from bone marrow cells using magnetic cell separation system (BD IMag Hematopoietic Progenitor Cell Enrichment Set-DM; BD Biosciences, San Jose, CA, http://www.bdbiosciences.com). In brief, cells isolated by centrifugation with low-density solution (<1.077 g/ml) were stained with a mixture of biotinylated mouse lineage-antibodies to CD3e, CD11b, CD45R/B220, Ly-6G and Ly-6C (Gr-1), and TER-119/erythroid cells (Ly-76). Lineage-positive cells were depleted with streptavidin–magnetic beads and the use of neodymium magnets (BD IMagnet; BD Biosciences). The remaining cells were collected and further stained with phycoerythrin-conjugated anti-Sca-1 and allophycocyanin-conjugated anti-c-Kit antibodies. All antibodies were purchased from BD Biosciences. After washing, the cells were resuspended in staining medium supplemented with 7-amino-actinomycin D (7-AAD). Stained cells were analyzed by fluorescence activated cell sorting (FACS) using BD FACSAria cell-sorting system (BD Biosciences), and KSL cells were sorted. Dead cells stained with 7-AAD were excluded from analysis and sorting.

EPC Colony Forming Assay

An EPC colony forming assay established in our laboratory was performed as reported previously [15]. The number of EPC colonies was assessed after culturing single-KSL cells in a 96-well plate for 12 days in methyl cellulose-containing medium M3236 (StemCell Technologies, Vancouver, BC, Canada, http://www.stemcell.com) with 20 ng/ml SCF (Kirin, Tokyo, Japan, http://www.kirin.co.jp/english), 50 ng/ml vascular endothelial growth factor (VEGF) (R&D Systems, Minneapolis, MN, http://www.rndsystems.com), 20 ng/ml interleukin-3 (Kirin), 50 ng/ml basic fibroblastic growth factor (Wako, Osaka, Japan, http://www.wako-chem.co.jp/english), 50 ng/ml epidermal growth factor (EGF) (Wako), 50 ng/ml insulin-like growth factor-1 (IGF-1) (Wako), and 2U/ml heparin (Ajinomoto, Tokyo, Japan, http://www.ajinomoto.com). Results were expressed as mean ± SD. Statistical analysis was performed using the Mann-Whitney U test. The endothelial phenotype of the EPC colonies was confirmed by high uptake of DiI conjugated acetylated low-density lipoprotein (DiI-Ac-LDL; Biomedical Technologies, Stoughton, MA, http://www.btiinc.com), cytochemical positivity for Alexa Fluor 488 conjugated Isolectin B4 (Molecular Probes, Carlsbad, CA, http://probes.invitrogen.com), immunoreactivity for Flk-1 (Sigma, St. Louis, MO, http://www.sigmaaldrich.com), and eNOS (Sigma).

SCI Model

All surgical procedures were performed using an operating microscope (Zeiss, Oberkochen, Germany, http://www.zeiss.com). Male C57BL/6 mice (12 weeks old, weighing 24-26g) were anesthetized with an intraperitoneal injection of 400 mg/kg 2,2,2-tribromoethanol (Avertin; Sigma). After a laminectomy at the 10th thoracic spinal vertebrae, we exposed the dura mater. Spinal cord crush injury was performed by compressing the cord laterally from both sides with number 5 Dumont forceps (Fine Science Tools, North Vancouver, BC, Canada, http://www.finescience.com) as previously reported [16, 17]. In previous reports, the forceps were modified with a spacer so that a 0.4 or 0.5 mm space remained at maximal closure. These distances were selected for moderately severe injury by comparing results achieved with forceps that closed to a space of 1.0 or 0 mm. In the present study, we selected forceps without a spacer in order to make severe and reproducible injury models. Their bladders were emptied manually once a day until restoration of autonomic bladder function.

Transplantation of KSL Cells

Transplantation was performed immediately after spinal cord injury. KSL cells (1×10^5 cells in 200 μl of postbum serum (PBS)) derived from wild-type mice (WT KSL group) or Lnk knockout mice (Lnk KO KSL group) were injected intravenously. In the other injured mice, only 200 μl of PBS was injected (PBS group).

Behavioral Testing

The recovery of hindlimb motor function was assessed using the BBB locomotor rating scale [18]. Mice in each group (n = 10-12) were assessed before SCI and 1, 4, 7, 14, 21, 28, 35, and 42 days after injury. Mice were evaluated in an open field by two observers blind to the experimental condition. Results were expressed as mean ± standard error. Statistical analysis was performed using two-way repeated measures ANOVA for group × time and Scheffe's post hoc comparisons.

Electrophysiological Recording

Signal conduction in the motor pathway was assessed by motor evoked potentials (MEPs) at 6 weeks after injury as described previously [19]. Mice were anesthetized with an intraperitoneal injection of 100 mg/kg of ketamine hydrochloride, which has little effect on the MEP [20]. They were then fixed in a stereotaxic apparatus. A pair of needle electrodes was placed subcutaneously at 3 mm on each side of the vertex of the skull. The motor cortex was stimulated transcranially with 0.2 ms square wave pulses using a constant current of 50 mA. The electromuscular responses were recorded from both hamstring muscles using a commercially available system (Viking Quest; Nicolet Biomedical, Madison, WI, http://www.viasyshealthcare.com/). All signals were filtered (bandpass 0.5-2,000 Hz). To ensure reproducibility, at least five replicate responses were recorded and the recording with the highest amplitude from onset to peak of the negative deflection was used for analysis [21, 22]. Results were expressed as mean ± SD. Statistical analysis was performed using one-way ANOVA followed by Scheffe's post hoc comparisons.

Immunohistochemistry

Mice were anesthetized and transcardially perfused with 4% paraformaldehyde in PBS at day 1, 3, 14, and 42 after injury. Spinal

cords were frozen and sagittally sectioned at 16 μm on a cryostat. Sections were permeabilized with 0.3% TritonX-100 and non-specific binding sites were blocked with blocking solution (Protein Block Serum-Free; Dako, Carpinteria, CA, http://www.dako.com). Where anti-mouse IgG monoclonal antibodies were used, sections were additionally incubated with mouse IgG blocking reagent (Vector Laboratories, Burlingame, CA, http://www.vectorlabs.com). Spinal cord sections were stained with the following primary antibodies: mouse anti-nestin (1:100; BD Biosciences), rabbit anti-GFAP (1:500; Dako), rabbit anti-collagen type IV (1:200; LSL, Tokyo, Japan, http://www.cosmobio.co.jp/agency/z01.asp), rabbit anti-tyrosine hydroxylase (TH; 1:500, Chemicon, Temecula, CA, http://www.chemicon.com), rat anti-CD31 (1:100; Santa Cruz Biotechnology, Santa Cruz, CA, http://www.scbt.com), goat anti-serotonin transporter (5HT; 1:500; ImmunoStar, Hudson, WI, http://www.immunostar.com) and Alexa Fluor 488 conjugated anti-green fluorescent protein (GFP) (1:500; Molecular Probes). Secondary antibodies (1:500) used were as follows: Alexa Fluor 488 conjugated goat anti-mouse (Molecular Probes), Alexa Fluor 594 conjugated goat anti-mouse, Alexa Fluor 350 conjugated goat anti-rabbit, Alexa Fluor 488 conjugated goat anti-rabbit, Alexa Fluor 488 conjugated donkey anti-rabbit, Alexa Fluor 594 conjugated goat anti-rabbit, Alexa Fluor 594 conjugated donkey anti-rat, and Alexa Fluor 594 donkey anti-goat. Finally, except for those stained with Alexa Fluor 350 conjugated secondary antibody, the tissues were counterstained with DAPI. Immunostained sections were observed under a fluorescence microscope (BZ8000; Keyence, Osaka, Japan, http://www.keyence.com).

For the quantitative assessment of axons, the area of TH^+ or $5HT^+$ axons at two levels (caudal region adjacent to the epicenter and 5 mm caudal to the epicenter) was measured using ImageJ software as previously described [23, 24]. The diameter, number, and area of $CD31^+$ vessels, the number of $GFAP^+$ cells, GFAP negative area, and Collagen type IV^+ area were also measured by ImageJ for quantitative assessment [25, 26]. Results were expressed as mean ± SD. Statistical analysis was performed using the Mann-Whitney U test (in the case of comparison between only two groups) or one-way ANOVA followed by Scheffe's post hoc comparisons (in the case of multiple comparisons).

Real-Time Polymerase Chain Reaction Analysis in KSL Cells and Injured Spinal Cord Tissues

Total RNA was obtained from $Lnk^{+/+}$ KSL cells and $Lnk^{-/-}$ KSL cells using RNeasy Mini Kit (Qiagen KK, Tokyo, Japan, http://www1.qiagen.com) according to the manufacturer's procedure. Total RNA from spinal cord tissues was also obtained as previously described [27]. At day 3 after SCI, mice were anesthetized and transcardially perfused with 15 ml of sterile RNase-free PBS. Spinal cords were rapidly dissected, and a 5 mm segment centered on the lesion was removed and homogenized in Trizol (Invitrogen, Carlsbad CA, http://www.invitrogen.com). RNA was isolated according to the manufacturer's protocol. After the first-strand cDNA was synthesized with the use of PrimeScript RT reagent Kit (TaKaRa, Otsu, Japan, http://www.takara.co.jp), real-time quantitative reverse transcription-polymerase chain reaction (RT-PCR) was performed with ABI Prism 7,700 (Applied Biosystems, Foster City, CA, http://www.appliedbiosystems.com) using SYBR Green Master Mix reagent (Applied Biosystems) according to the manufacturer's protocol. The relative mRNA expression in each gene was normalized to the expression level of glyceraldehyde-3-phosphate dehydrogenase (GAPDH). In this method of calculation, expression level of GAPDH was reduced to 10,000. Results were expressed as mean ± SD. Statistical analysis was performed using the Mann-Whitney U test (in the case of comparison between only two groups) or one-way ANOVA followed by Scheffe's post hoc comparisons (in the case of multiple comparisons). Each primer sequence is shown in supporting information Table 1.

Results

EPC Colony Forming Units from KSL Cells

Flow cytometric analysis revealed that the ratio of $c\text{-}Kit^+$ and $Sca\text{-}1^+$ cells in the $lineage^-$ bone marrow mononuclear cell fraction isolated from Lnk knockout mice (21.8 ± 2.0%) was significantly higher than in control wild-type mice (7.7 ± 3.1%), as already shown in our previous report (Fig. 1A) [10]. To evaluate the ability of KSL cells to function as EPCs in vitro, KSL cells derived from wild-type as well as Lnk knockout mice were analyzed by EPC colony-forming assay (Fig. 1B, 1C) [15]. EPC colonies formed from KSL cells exhibited endothelial properties, including uptake of acetylated low-density lipoprotein conjugated with DiI (DiI-acetyl LDL), chemical reactivity for Isolectin B4, and immunoreactivity for vascular endothelial growth factor (VEGF) receptor-2 (Flk-1) and endothelial nitroxide synthase (eNOS) (Fig. 1B). To assess colony formation from a single cell, KSL cells were cultured in 96-well plates (single cell per well). The average number of EPC colonies per plate from $Lnk^{-/-}$ KSL cells was significantly greater than from $Lnk^{+/+}$ KSL cells (Fig. 1C). These findings suggest that Lnk deletion increased the ability of KSL cells to function as EPCs in vitro.

Gene Expression Profiles in KSL Cells

The mRNA expressions of endothelial lineage markers, stem/progenitor cell mobilization factor receptors, growth factors, and cytokines were analyzed using quantitative real-time PCR (Fig. 2). The mRNA expression level in each gene was normalized to the expression level of GAPDH. In the assessment of endothelial lineage markers, the expression levels of endoglin (CD105), vascular endothelial-cadherin (VE-cadherin, CD144), Tie-1, and Tie-2 in $Lnk^{-/-}$ KSL cells were significantly higher than in $Lnk^{+/+}$ KSL cells (Fig. 2A). In the assessment of receptors for stem/progenitor cell mobilization factors, c-Kit was highly expressed compared to VEGF receptor-1 (Flt-1), Flk-1, and CXC chemokine receptor four, and the expression level of c-Kit in $Lnk^{-/-}$ KSL cells was significantly higher than in $Lnk^{+/+}$ KSL cells (Fig. 2B). In the assessment of growth factors and cytokines, comparatively low level expressions of VEGF-C, placenta growth factor (PlGF), insulin-like growth factor one (IGF1), IGF2, brain-derived growth factor (BDNF), stem cell factor (SCF), and stromal cell-derived factor one (SDF1) were observed, together with a high level of expression of angiopoietin one (Ang1). The expression level of Ang1 and SCF in $Lnk^{-/-}$ KSL cells was significantly higher than in $Lnk^{+/+}$ KSL cells (Fig. 2C).

Functional Recovery Following Spinal Cord Injury

To assess the functional capacity of KSL cells for the treatment of injured spinal cord, PBS, $Lnk^{+/+}$ KSL cells, as well as $Lnk^{-/-}$ KSL cells were administered intravenously to SCI models of wild-type mice just after injury (PBS group, WT KSL group, and Lnk KO KSL group). The recovery of hindlimb function was assessed by using the BBB locomotor rating scale [18]. The sham control mice had scores of 21 in the BBB locomotor rating scale. All mice in PBS group, WT KSL group, and Lnk KO KSL group had a score of 21 (maximum score) before SCI, with the score being reduced to 0 at 1 day after SCI (n = 10-12 per group). Significant group effects were identified with repeated measures ANOVA ($p < .0001$ group, time and group × time interaction). The BBB

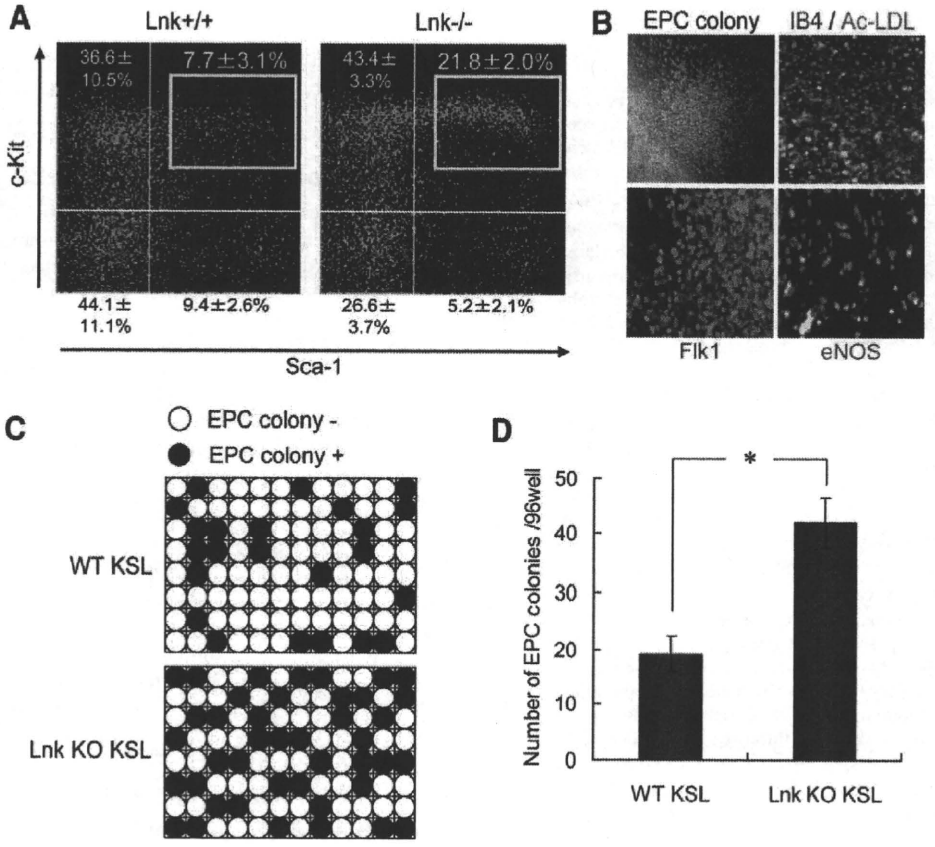

Figure 1. (**A**): Flow cytometric analysis. Expression of c-Kit and Sca-1 in Lineage$^-$ bone marrow mononuclear cells from wild-type mouse and Lnk knockout mouse. (**B**): Pictures of EPC colonies. Endothelial character of EPC colony cells was confirmed by uptake of DiI-acetyl LDL, chemical reactivity to Isolectin B4, and immunoreactivity for Flk-1 and eNOS. (**C, D**): EPC colony forming assay in bone marrow KSL cells from wild-type mice (WT KSL) and Lnk knockout mice (Lnk KO KSL). Schematic diagrams of representative EPC colony forming patterns (**C**) and graph of the number of EPC colonies per 96-well plate (**D**). *, Significant difference, $p < .05$. Abbreviations: Ac-LDL, acetylated low-density lipoprotein; eNOS, endothelial nitroxide synthase; EPC, endothelial progenitor cell; KO, knockout; KSL, c-Kit positive, Sca-1 positive, lineage marker-negative; WT, wild-type.

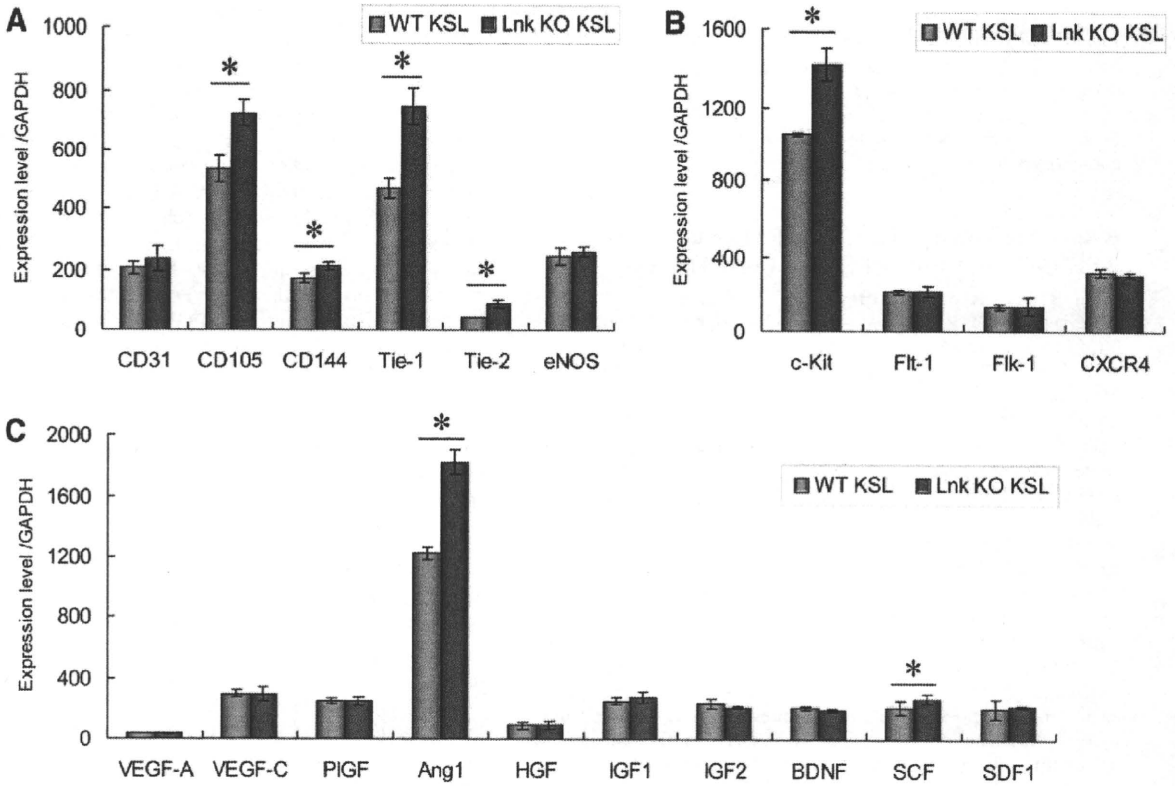

Figure 2. Gene expression profiles of bone marrow KSL cells from wild-type mice (WT KSL) and Lnk knockout mice (Lnk KO KSL) measured by real-time polymerase chain reaction. (**A**): mRNA expressions of endothelial lineage markers, including CD31, CD105, CD144, Tie-1, Tie-2, and eNOS. (**B**): mRNA expressions of receptors for stem/progenitor cell mobilization factors, including c-Kit, Flt-1, Flk-1, and CXCR4. (**C**): mRNA expressions of growth factors and cytokines, including VEGF-A, VEGF-C, PlGF, Ang1, HGF, IGF1, IGF2, BDNF, SCF, and SDF1. *, Significant difference, $p < .05$. Abbreviations: Ang, angiopoietin; BDNF, brain-derived growth factor; CXCR, CXC chemokine receptor; eNOS, endothelial nitroxide synthase; GAPDH, glyceraldehyde-3-phosphate dehydrogenase; HGF, hepatocyte growth factor; IGF, insulin-like growth factor; KO, knockout; KSL, c-Kit positive, Sca-1 positive, lineage marker-negative; PlGF, placenta growth factor; SCF, stem cell factor; SDF, stromal cell-derived factor; VEGF, vascular endothelial growth factor; WT, wild-type.

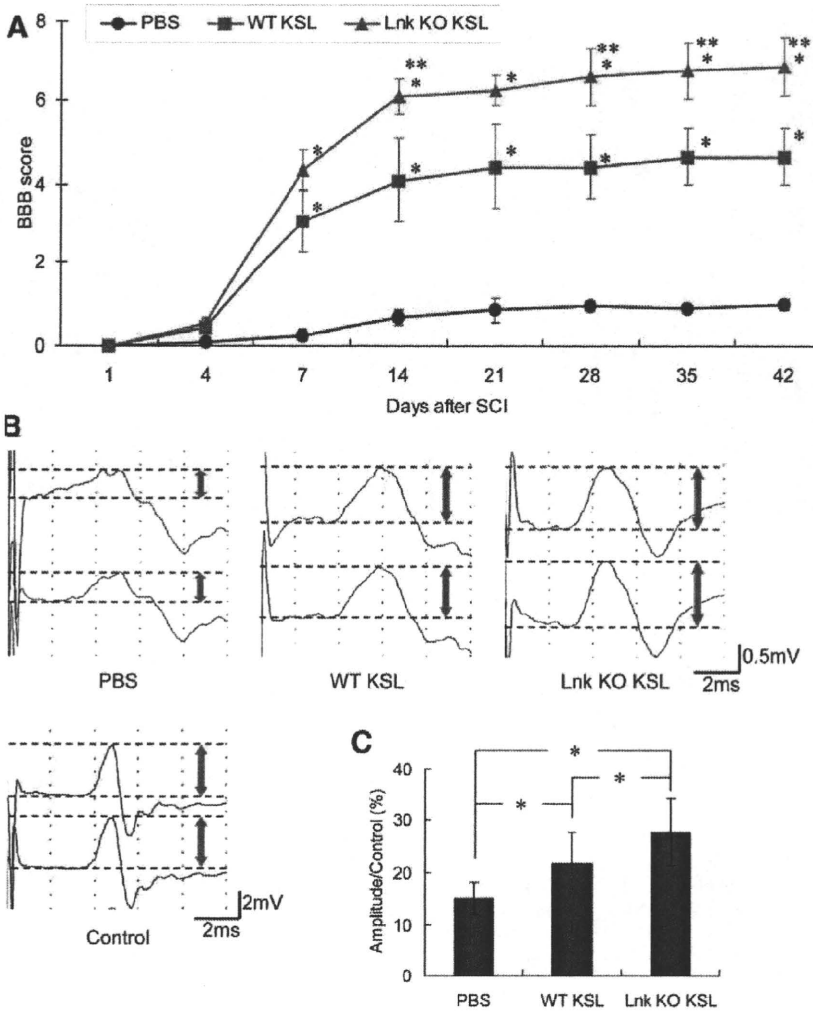

Figure 3. Assessment of functional recovery following spinal cord injury (n = 10-12). (**A**). Time course of functional recovery of limbs assessed using BBB locomotor rating scale. Significantly higher than * PBS group and ** WT KSL group, $p < .05$. (**B**). Representative motor evoked potential (MEP) waves at 6 weeks after injury. Amplitudes from onset to peak of the negative deflection were measured. (**C**): Relative ratio of MEP amplitudes to before injury. *, Significant difference, $p < .05$. Abbreviations: KO, knockout; KSL, c-Kit positive, Sca-1 positive, lineage marker-negative; PBS, postburn serum; SCI, spinal cord injury; WT, wild-type.

score in the WT KSL group and Lnk KO KSL group was significantly higher than in the PBS group at day 7 or later after SCI. In addition, the BBB score in the Lnk KO KSL group was significantly higher than in the WT KSL group at days 14, 28, or later after SCI (Fig. 3A). Hindlimb motor function while walking at days 1 and 28 after injury is shown in supporting information movies.

To assess functionality and recovery of descending pathways from the forebrain to the hindlimb motor neuron pool, transcranial electric motor evoked potentials (MEPs) were monitored in the hamstring muscles as previously reported [19]. Before SCI, MEPs were detected with an amplitude of 8.1 ± 2.0 mV (Pre-SCI; data not shown). At 6 weeks after SCI, the amplitude of MEPs in the PBS group, WT KSL group, and Lnk KO KSL group were 15.0 ± 3.1%, 21.6 ± 5.9%, and 27.7 ± 6.5% of the Pre-SCI values, respectively. The amplitude in the WT KSL group and Lnk KO KSL group was significantly higher than in the PBS group. Additionally, the amplitude in the Lnk KO KSL group was significantly higher than in the WT KSL group (Fig. 3B, 3C). These data indicate that transplantation of KSL cells facilitated the improvement of spinal cord function and that Lnk deletion enhanced the potential of KSL cells to improve the function of injured spinal cord even further.

Incorporation of Transplanted KSL Cells

To assess the incorporation of KSL cells systemically administered into mice with an injured spinal cord, KSL cells derived from GFP transgenic wild-type as well as Lnk knockout mice were administered to SCI models (n = 6/group). Spinal cord sections at 1, 3, and 14 days after SCI were analyzed under a fluorescence microscope (Fig. 4). At 1 day after SCI, GFP positive cells were detected only at the edge of spinal cord tissues around the injury site both in the WT KSL (Fig. 4B) and the Lnk KO KSL groups (Fig. 4C), although no cells were detected in the PBS group (Fig. 4A). At 3 days after SCI, GFP positive cells were detected in the spinal cord parenchyma around the injury site. A large portion of GFP^+ cells were incorporated into the platelet endothelial cell adhesion molecule-1 (PECAM-1, CD31) positive vessels or located along the $CD31^+$ vessels both in the WT KSL (Fig. 4D) and Lnk KO KSL groups (Fig. 4E). The number of GFP^+ cells in the Lnk KO KSL group was significantly greater than in the WT KSL group (Fig. 4F). At 14 days after SCI, no GFP^+ cells were observed in the spinal cord tissues from any of the groups (data not shown). Assessment of mRNA expression of stem/progenitor cell mobilization factors in the spinal cord tissues at day 3 after SCI (n = 3 per group) revealed that there was no significant difference in the

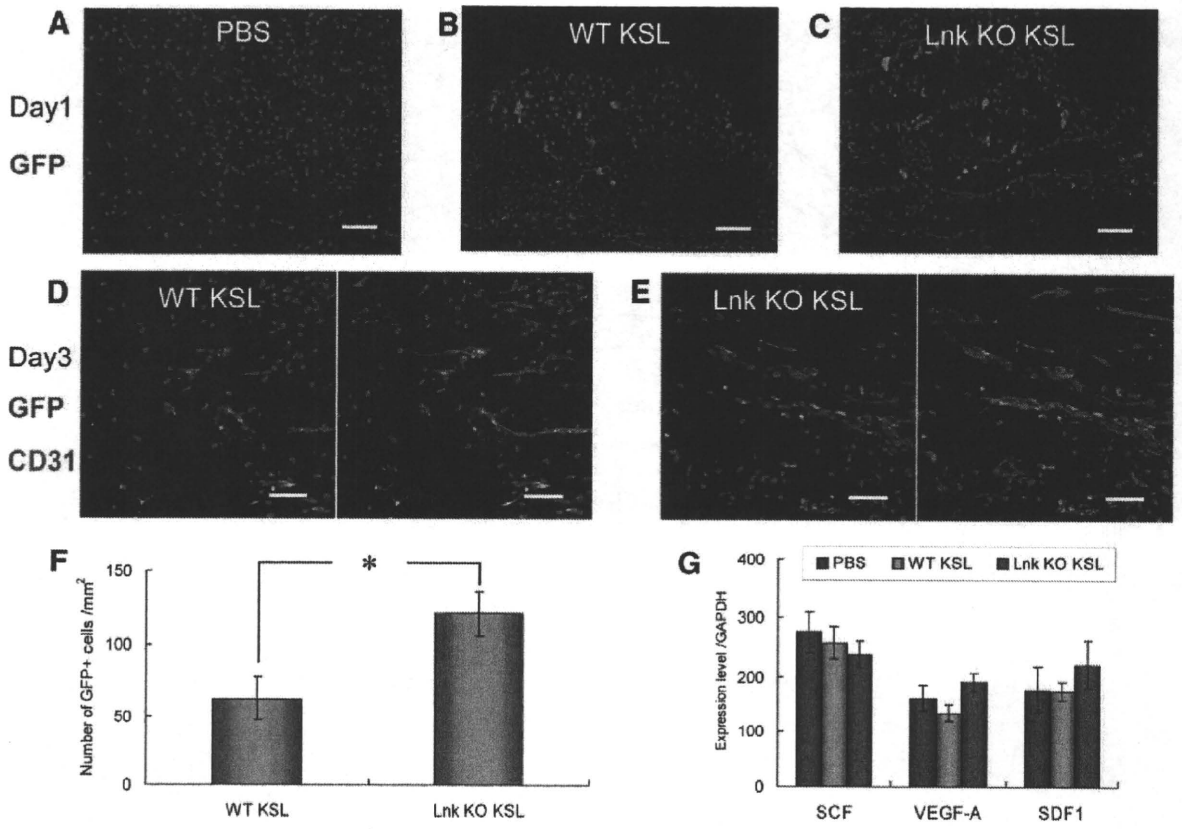

Figure 4. Incorporation of transplanted GFP$^+$ KSL cells into spinal cord. (**A**–**C**): Spinal cord tissues immunostained with anti-green fluorescent protein (GFP) antibodies at day 1 after injury in PBS group (**A**), WT KSL group (**B**), and Lnk KO KSL group (**C**). (**D**, **E**): Spinal cord tissues immunostained with anti-GFP and anti-CD31 antibodies at day 3 after injury in WT KSL group (**D**) and Lnk KO KSL group (**E**). (**F**): Number of GFP$^+$ cells incorporated into spinal cord at day 3 after injury. (**G**): mRNA expressions of stem/progenitor cell mobilization factors, including stem cell factor, vascular endothelial growth factor-A, and stromal cell-derived factor one in spinal cord tissues at day 3 after injury. *, Significant difference, $p < .05$. Scale bar: (**A**–**E**): 50 μm. Abbreviations: GFP, green fluorescent protein; KO, knockout; KSL, c-Kit positive, Sca-1 positive, lineage marker-negative; PBS, postburn serum; WT, wild-type.

expression levels of SCF, VEGF, and SDF1 among the PBS, WT KSL, and Lnk KO KSL groups (Fig. 4G).

Neovascularization and Astrogliosis in Injured Spinal Cord

At day 3 after SCI, the diameter, number, and area of CD31$^+$ vessels were analyzed in the region adjacent to the epicenter of the injury site (dotted-line box in Fig. 4A). The mean diameter, number, and area of vessels in the WT KSL and Lnk KO KSL groups were significantly larger than in the PBS group. Although the number of vessels in the Lnk KO KSL group was similar to that in the WT KSL group, the mean diameter and area of vessels in the Lnk KO KSL group were significantly greater than those in the WT KSL group (Fig. 5A, 5B). At day 3 after SCI, reactive astrocytes were stained with antibodies against glial fibrillary acidic protein (GFAP; green in Fig. 5C) and nestin (red in Fig. 5C). Reactive astrocytes were detected around the injury site (dotted-line box in Fig. 5C) both in WT KSL and Lnk KO KSL groups, whereas they were rare in the PBS group (Fig. 5C). In Figure 5C, some GFAP$^+$ astrocytes in the sections are nestin negative. Because nestin is a marker for immature cell, we speculate that GFAP$^+$ and nestin$^-$ cells might involve remaining astrocytes after injury or matured reactive astrocytes. A large portion of reactive astrocytes were distributed along large CD31$^+$ vessels (Fig. 5D). The number of reactive astrocytes in the WT KSL and Lnk KO KSL groups was significantly greater than that in the PBS group. Additionally, the number of reactive astrocytes in the Lnk KO KSL group was significantly greater than that in the WT KSL group (Fig. 5E). These findings suggest that transplantation of KSL cells promotes angiogenesis and astrogliosis in the acute phase of spinal cord injury and that Lnk deletion strengthens the function of KSL cells in promoting these events.

At day 14 after injury, morphological changes of CD31$^+$ vessels at the epicenter of the injury site (epicenter zone; area 1 in Fig. 5A) were different from ones of the laterally-damaged region (lateral zone; area 2 in Fig. 5A). Therefore, the diameter, number, and area of CD31$^+$ vessels in these regions were assessed separately ($n = 6$ per group). In the epicenter zone, a chaotic vascular architecture with large vessels adjacent to small vessels was observed in the PBS group (Fig. 6C). In contrast, the diameter and distribution of vessels in the WT KSL and Lnk KO KSL groups resembled the distribution found in the gray matter of normal spinal cord (Fig. 6B, 6C). The mean diameter, number, and area of CD31$^+$ vessels in the PBS group were significantly greater than in the normal spinal cords, the WT KSL, and the Lnk KO KSL groups (Fig. 6E–6G). Although there was no significant difference in the mean diameter of vessels between the WT KSL and Lnk KO KSL groups, the mean diameter of vessels in the WT KSL group was significantly larger than in the normal spinal cord, whereas the mean diameter of vessels in the Lnk

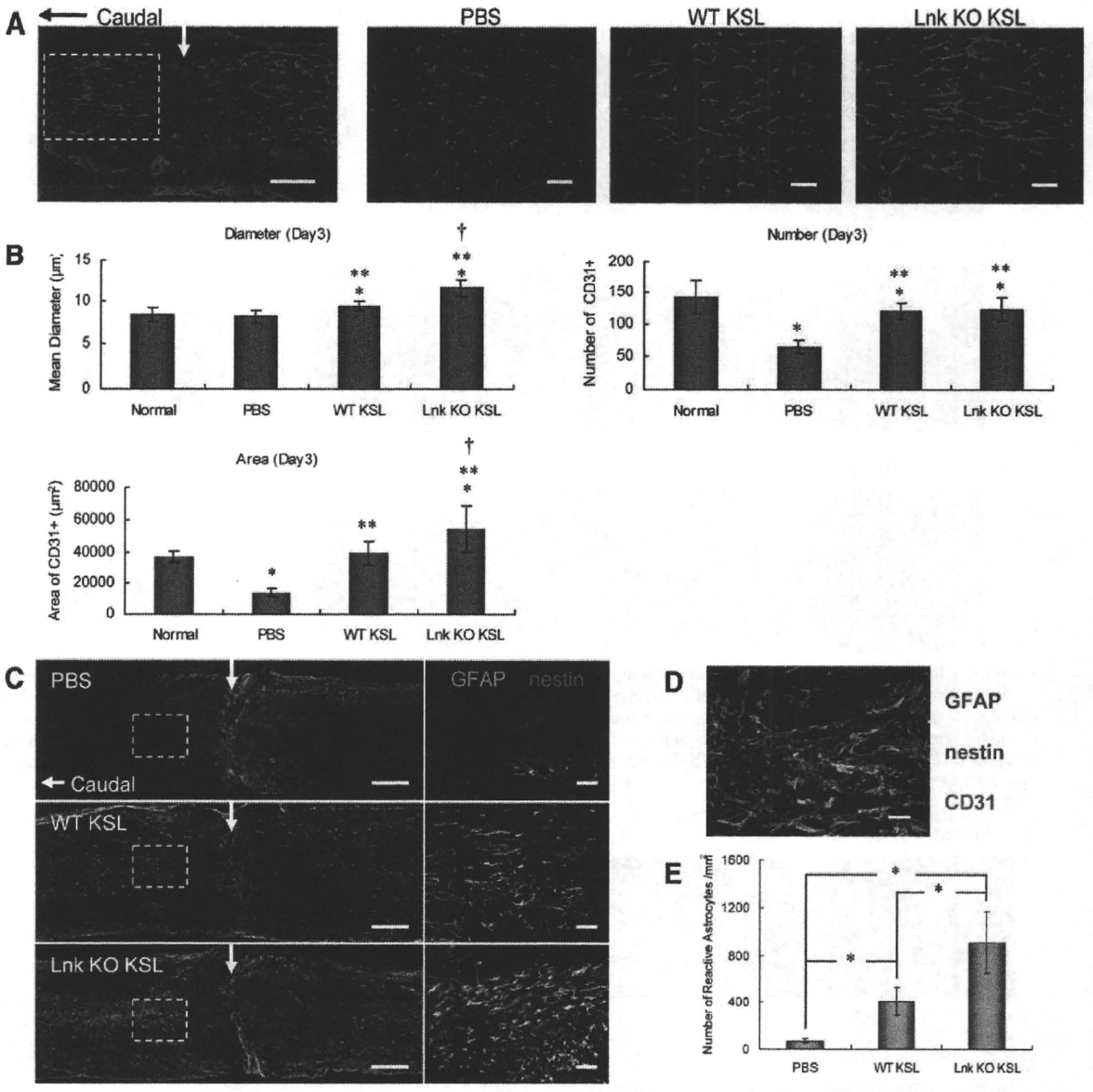

Figure 5. **(A)**: Spinal cord sections at day 3 after injury immunostained with CD31. Arrow indicates epicenter of injury site. **(B)**: Assessment of mean diameter, number, and area of $CD31^+$ vessels ($n = 6$). **(C)**: Spinal cord tissues at day 3 after injury immunostained with GFAP (green) and nestin (red). **(D)**: Spinal cord section at day 3 after injury immunostained with GFAP (blue), nestin (green), and CD31 (red) in Lnk KO KSL group. **(E)**: Number of $GFAP^+$ cells at day 3 after injury ($n = 6$). Significantly different from * non-injured spinal cord, ** PBS group, and † WT KSL group, $p < .05$. Scale bars: **(A)**: Large picture, 300 μm, and small pictures, 100 μm; **(C)**: Large pictures, 300 μm, and small pictures, 50 μm; **(D)**: 20 μm. Abbreviations: GFAP, glial fibrillary acidic protein; KO, knockout; KSL, c-Kit positive, Sca-1 positive, lineage marker-negative; PBS, postburn serum; WT, wild-type.

KO KSL group was not significantly different from that of the normal spinal cord (Fig. 6E). In the lateral zone, there were no obviously large vessels observed in the epicenter zone (Fig. 6D). The mean diameter of vessels in the Lnk KO KSL group was significantly larger than in the PBS group, although not significantly different from the normal spinal cord (Fig. 6E). The number of vessels in the WT KSL group was significantly less than in normal spinal cords, while the number of vessels in the Lnk KO KSL group was not significantly different from the number found in the normal spinal cords but was significantly greater than that in the WT KSL group (Fig. 6F). The area of vessels in the PBS group was significantly smaller than that in the normal spinal cord, where as the area of vessels in the Lnk KO KSL group was significantly larger than that in the PBS group and the WT KSL group (Fig. 6G). These findings suggest that the transplantation of KSL cells contributes to vascular stabilization at the epicenter of the injury site in the subacute phase of SCI and that Lnk deletion enhances the function of KSL cells for vascular stabilization in the epicenter zone even further, promoting angiogenesis in the lateral zone during the subacute phase of SCI.

At day 42 after SCI, spinal cord tissues were stained with antibodies against GFAP and collagen type IV for the assessment of glial and fibrous scar formation ($n = 6$ per group, Fig. 7). The GFAP negative area in the WT KSL group and

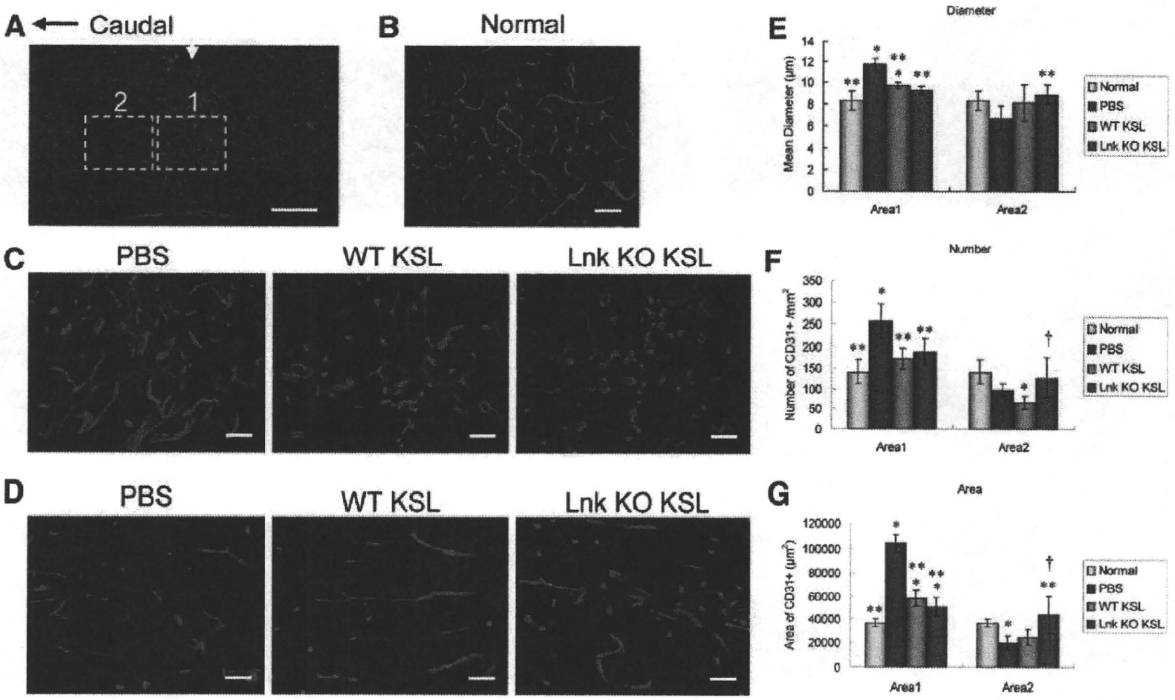

Figure 6. Immunostaining for CD31 in non-injured spinal cord and injured spinal cord at day 14 after injury. **(A)**: CD31$^+$ vessels were assessed at the epicenter of the injury site (epicenter zone, Area1) and the laterally damaged region (lateral zone, Area2). **(B)**: Gray matter in non-injured spinal cord (Normal). **(C)**: Area1 in the injured spinal cord. **(D)**: Area2 in the injured spinal cord. **(E–G)**: Quantitative assessment of vessels, including mean diameter **(E)**, number **(F)**, and area **(G)**. Significantly different from * non-injured spinal cord, ** PBS group, and †WT KSL group, $p < .05$. Scale bars: **(A)**: 300 μm; **(B–D)**: 50 μm. Abbreviations: KO, knockout; KSL, c-Kit positive, Sca-1 positive, lineage marker-negative; PBS, postburn serum; WT, wild-type.

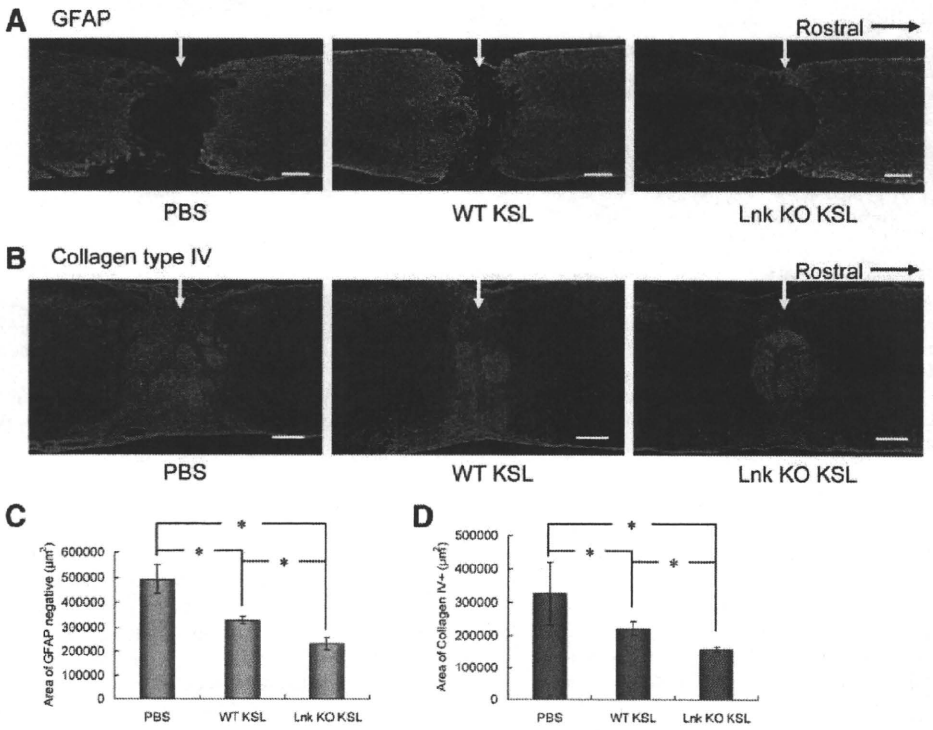

Figure 7. **(A, B)**: Spinal cord sections immunostained with GFAP **(A)** and collagen type IV **(B)** at 6 weeks after injury. **(C, D)**: Quantitative assessment of GFAP negative area **(C)** and collagen type IV$^+$ area **(D)**. * Significant difference, $p < .05$. Scale bars: **(A, B)**: 300 μm. Abbreviations: GFAP, glial fibrillary acidic protein; KO, knockout; KSL, c-Kit positive, Sca-1 positive, lineage marker-negative; PBS, postburn serum; WT, wild-type.

the Lnk KO KSL group was significantly smaller than that in the PBS group. Furthermore, the GFAP-negative area in the Lnk KO KSL group was significantly smaller than that in the WT KSL group (Fig. 7A, 7C). In the assessment of the collagen IV$^+$ area, a similar pattern compared to the GFAP-negative area was observed (Fig. 7B, 7D).

Immunohistochemical Assessment of Axons

To analyze defined subsets of descending axons, immunohistochemistry for tyrosine hydroxylase (TH; a marker for descending noradrenergic and dopaminergic axons as well as sympathetic fibers) and serotonin transporter (5HT; a marker for descending serotonergic axons) was performed as previously reported [28]. To evaluate axon growth into the injury site, quantitative assessment of axons was performed by measuring the area of immunostained axons in the caudal region adjacent to the epicenter of the injury site (dotted-line box in supporting information Fig. 1A, 1B). The area of TH^+ or $5HT^+$ axons in the WT KSL and Lnk KO KSL groups was significantly greater than that in the PBS group. In addition, the area of TH^+ or $5HT^+$ axons in the Lnk KO KSL group was significantly greater than that in the WT KSL group (supporting information Fig. 1C, 1D). A similar assessment of axons was also performed in the far caudal region (5 mm caudal to the epicenter). However, neither TH^+ axons nor $5HT^+$ axons were detected in any of the groups analyzed (data not shown).

Discussion

Our findings demonstrate that the transplantation of KSL cells promotes angiogenesis and astrogliogenesis in the acute phase of SCI and vascular stabilization, reduction of fibrous scar formation, axonal growth and functional recovery in the subacute phase and later. Lnk deletion enhances the effect of KSL cell transplantation even further, promoting regenerative changes in the injured spinal cord.

Lnk Deletion Enhances the Potential of KSL Cells As EPCs

Lnk was reported to negatively regulate SCF/c-Kit signaling in B cell progenitors, hematopoietic stem/progenitor cells, and mast cells [10, 13, 29]. Lnk is furthermore considered to negatively regulate endothelial cell derived hematopoiesis during embryonic development [30]. In addition, Lnk is expressed in endothelial cells and played a role in the regulation of vascular cell adhesion molecule-1 expression in response to tumor necrosis factor-α through inhibition of the extracellular-related kinase 1/2 pathway [31, 32]. On the basis of these data, we speculate that Lnk might be involved in the differentiation and functional regulation of endothelial cells as well as endothelial progenitor cells [33]. In the present study, the mRNA expression levels of several endothelial markers in $Lnk^{-/-}$ KSL cells were higher than in $Lnk^{+/+}$ KSL cells. In addition, Lnk deletion enhanced the EPC colony forming potential of KSL cells in vitro. In vivo, the transplantation of $Lnk^{-/-}$ KSL cells further promoted angiogenesis compared to $Lnk^{+/+}$ KSL cells. These findings indicate that Lnk deletion intensified the ability of KSL cells to function as EPCs. Lnk might negatively regulate the proliferation of EPCs or the commitment of bone marrow stem cells to EPCs, although further elucidation of the role of Lnk in EPCs is needed.

Recruitment of Transplanted KSL Cells into Injured Spinal Cord

The mRNA expression level of c-Kit, which is a receptor for SCF in $Lnk^{-/-}$ KSL cells, was significantly higher than in $Lnk^{+/+}$ KSL cells. We validated this observation by showing that $Lnk^{-/-}$ KSL cells contained a bigger $c\text{-}Kit^+$ fraction than $Lnk^{+/+}$ KSL cells by flow cytometric assessment (Fig. 1A). On the other hand, no significant difference in the mRNA expression levels of SCF, VEGF, and SDF1 were observed in the injured spinal cord tissues of all three analyzed groups. SCF is believed to play an important role not only for proliferation and survival but also in the homing of hematopoietic progenitor cells [34]. Lutz et al. reported that myocardial administration of SCF-enhanced myocardial recruitment of intravenously injected bone marrow $c\text{-}Kit^+$ $lineage^-$ cells [35]. In analogy, the higher expression of c-Kit in $Lnk^{-/-}$ KSL compared to $Lnk^{+/+}$ KSL cells may explain the observed high incorporation of administered $Lnk^{-/-}$ KSL cells into the injured spinal cord.

KSL Cells Enhance the Angiogenesis in the Acute Phase of SCI

At day 3 after SCI, angiogenesis was enhanced by the transplantation of KSL cells. The mRNA expressions of several angiogenic factors, including VEGF-C, PlGF, Angl, IGF1, IGF2, and BDNF, were observed in KSL cells. In particular, the expression level of Angl was strikingly higher than any of the other factors. A previous study showed that a balanced expression of Angl and VEGF is required for successful angiogenesis [36]. We therefore speculate that Angl might be a key factor for the induction and enhancement of angiogenesis after KSL cell transplantation. In addition, the expression level of Angl in $Lnk^{-/-}$ KSL cells was significantly higher than in $Lnk^{+/+}$ KSL cells. Overall, the high incorporation of $Lnk^{-/-}$ KSL cells into injured spinal cord together with a high expression of Angl in $Lnk^{-/-}$ KSL cells might be the cause for the strong induction of angiogenesis seen after $Lnk^{-/-}$ KSL cell transplantation.

KSL Cells Promote Astrogliosis Following SCI

Glial scars, formed in part by reactive astrocytes after SCI, have long been considered detrimental to the repair of injured spinal cord because glial scars or their products act as physical or chemical barriers to axonal regeneration [37–39]. However, recent studies have shown that reactive astrocytes are also important in supporting the repair of injured spinal cord [16, 25, 40]. They mentioned that reactive astrocytes are important for the repair of the blood–brain barrier and the restriction of inflammation that leads to a reduction in secondary degeneration after SCI. In addition, it has been reported that various growth factors such as nerve growth factor, brain-derived growth factor (BDNF), hepatocyte growth factor, VEGF, and fibroblast growth factor-2, which promote neuroprotection, axonal growth, and angiogenesis, are expressed in reactive astrocytes [41]. On the basis of these data from previous studies, reactive astrocytes, at least in the acute and subacute phase of SCI, might be considered beneficial to the repair of the injured spinal cord. In the present study, the transplantation of KSL cells promoted the induction of reactive astrocytes following SCI. Furthermore, Lnk deletion enhanced the effect of KSL cell transplantation promoting astrogliogenesis following SCI. Additionally, particular localization of reactive astrocytes along large vessels was observed. Recent previous studies have shown that the vascular niche is closely related to the commitment of slow-proliferating neural stem cells to fast-proliferating transit-amplifying precursors in the adult subventricular zone in homeostasis as well as during regeneration, whereas molecular mechanisms underlying this phenomenon have not been clarified [42, 43]. We therefore speculate that the promotion of angiogenesis caused by the transplantation of KSL cells enhanced astrogliogenesis through the provision of a functional vascular niche.

KSL Cells Contribute to Vascular Stabilization in the Subacute Phase of SCI

In the present study, morphological vascular abnormalities, represented by an abnormally high number of vessels, many of which were enlarged, were observed at the epicenter of the injury site, which was devoid of astrocytes in the PBS group at day 14 after SCI. This abnormal pattern of vascular structures resembled abnormal vessels usually seen in tumors, CNS neurodegenerative diseases, or the injured brain, resulting in vascular hyperpermeability and blood–brain barrier dysfunction [26, 44, 45]. In the CNS, not only pericytes but also astrocytes are required for the formation of healthy blood vessels [45]. In contrast, the number and diameter of vessels in the spinal cord treated with KSL cells resembled the appearance of normal gray matter found in non-injured spinal cords. Angl is believed to play an important role not only in angiogenesis but also in vascular stabilization [46]. Ang-1 has also been shown to override VEGF-mediated effects on vascular permeability [47, 48]. In addition, overexpression of Angl stabilized tumor vessels and inhibited the growth of cancer [49, 50]. Therefore, we speculate that transplanted KSL cells contribute to vascular stabilization through Angl signaling and that Lnk deletion enhances these functions.

KSL Cells Reduce Fibrous Scar Formation and Promote Axonal Regeneration

In this study, fibrous scar tissue in the injury site was immunostained with collagen type IV, which is a major structural component of basement membrane deposits of fibrous scars in the injured CNS [51]. At 6 weeks after SCI, the area of the collagen type IV^{+} fibrous scar was reduced by the transplantation of KSL cells. In addition, these areas in the Lnk KO KSL group were smaller than those in the WT KSL group. On the basis of these data, we speculate that restricted infiltration of inflammatory cells caused by rapid migration of reactive astrocytes and vascular stabilization in the spinal cord treated with KSL cells might result in an overall reduction of the fibrous scar area.

On the other hand, axonal growth beyond the injury site was enhanced by the transplantation of KSL cells. In addition, Lnk deletion enhanced even further the function of KSL cells in promoting axon growth. Lesion scars are considered a major impediment for axon regeneration in the injured CNS [52]. In particular, fibrous scars are associated with axonal growth inhibitory molecules such as chondroitin sulfate proteoglycans, semaphorins, and ephrins [24, 38, 53, 54]. Therefore, a reduction in fibrous scar area might have been involved in the enhancement of the axonal growth observed in the present study. We could not detect long tract regeneration of either dopaminergic axons or serotonergic axons in this study. Recent studies have reported that regenerating local axons can form intraspinal neural circuits in the lesion site after SCI and make synaptic connections with descending-tract collaterals [55, 56]. The signal relay mechanism via short regenerated neuronal fibers might be responsible for the functional recovery seen in the present study.

Acknowledgments

We would like to thank Akira Oyamada for technical support. We would like to express our appreciation to the animal facility of RIKEN Center for Developmental Biology for the use of their facilities.

This work was supported by a grant-in-aid for scientific research from the Uehara Memorial Foundation.

Disclosure of Potential Conflicts of Interest

References

1 Okada S, Nakauchi H, Nagayoshi K et al. In vivo and in vitro stem cell function of c-kit- and Sca-1-positive murine hematopoietic cells. Blood 1992;80:3044–3050.
2 Sata M, Saiura A, Kunisato A et al. Hematopoietic stem cells differentiate into vascular cells that participate in the pathogenesis of atherosclerosis. Nat Med 2002;8:403–409.
3 Bailey AS, Jiang S, Afentoulis M et al. Transplanted adult hematopoietic stems cells differentiate into functional endothelial cells. Blood 2004;103:13–19.
4 Sahara M, Sata M, Matsuzaki Y et al. Comparison of various bone marrow fractions in the ability to participate in vascular remodeling after mechanical injury. Stem Cells 2005;23:874–878.
5 Asahara T, Murohara T, Sullivan A et al. Isolation of putative progenitor endothelial cells for angiogenesis. Science 1997;275:964–967.
6 Taguchi A, Soma T, Tanaka H et al. Administration of CD34+ cells after stroke enhances neurogenesis via angiogenesis in a mouse model. J Clin Invest 2004;114:330–338.
7 Zhao ZM, Li HJ, Liu HY et al. Intraspinal transplantation of CD34+ human umbilical cord blood cells after spinal cord hemisection injury improves functional recovery in adult rats. Cell Transplant 2004;13:113–122.
8 Koshizuka S, Okada S, Okawa A et al. Transplanted hematopoietic stem cells from bone marrow differentiate into neural lineage cells and promote functional recovery after spinal cord injury in mice. J Neuropathol Exp Neurol 2004;63:64–72.
9 Koda M, Okada S, Nakayama T et al. Hematopoietic stem cell and marrow stromal cell for spinal cord injury in mice. Neuroreport 2005;16:1763–1767.
10 Takaki S, Morita H, Tezuka Y et al. Enhanced hematopoiesis by hematopoietic progenitor cells lacking intracellular adaptor protein, Lnk. J Exp Med 2002;195:151–160.
11 Seita J, Ema H, Ooehara J et al. Lnk negatively regulates self-renewal of hematopoietic stem cells by modifying thrombopoietin-mediated signal transduction. Proc Natl Acad Sci U S A 2007;104:2349–2354.
12 Bersenev A, Wu C, Balcerek J et al. Lnk controls mouse hematopoietic stem cell self-renewal and quiescence through direct interactions with JAK2. J Clin Invest 2008;118:2832–2844.
13 Takaki S, Sauer K, Iritani BM et al. Control of B cell production by the adaptor protein Lnk. Definition of a Conserved Family of Signal-Modulating Proteins. Immunity 2000;13:599–609.
14 Osawa M, Hanada K, Hamada H et al. Long-term lymphohematopoietic reconstitution by a single CD34-low/negative hematopoietic stem cell. Science 1996;273:242–245.
15 Kwon SM, Eguchi M, Wada M et al. Specific Jagged-1 signal from bone marrow microenvironment is required for endothelial progenitor cell development for neovascularization. Circulation 2008;118:157–165.
16 Faulkner JR, Herrmann JE, Woo MJ et al. Reactive astrocytes protect tissue and preserve function after spinal cord injury. J Neurosci 2004;24:2143–2155.
17 Herrmann JE, Imura T, Song B et al. STAT3 is a critical regulator of astrogliosis and scar formation after spinal cord injury. J Neurosci 2008;28:7231–7243.
18 Basso DM, Beattie MS, Bresnahan JC. A sensitive and reliable locomotor rating scale for open field testing in rats. J Neurotrauma 1995;12:1–21.
19 Yamada K, Tanaka N, Nakanishi K et al. Modulation of the secondary injury process after spinal cord injury in Bach1-deficient mice by heme oxygenase-1. J Neurosurg Spine 2008;9:611–620.
20 Ghaly RF, Stone JL, Aldrete JA et al. Effects of incremental ketamine hydrochloride doses on motor evoked potentials (MEPs) following transcranial magnetic stimulation: A primate study. J Neurosurg Anesthesiol 1990;2:79–85.
21 García-Alías G, Lopez-Vales R, Fores J et al. Acute transplantation of olfactory ensheathing cells or Schwann cells promotes recovery after spinal cord injury in the rat. J Neurosci Res 2004;75:632–641.

22 Kim JE, Liu BP, Park JH et al. Nogo-66 receptor prevents raphespinal and rubrospinal axon regeneration and limits functional recovery from spinal cord injury. Neuron 2004;44:439–451.
23 Takami T, Oudega M, Bates ML et al. Schwann cell but not olfactory ensheathing glia transplants improve hindlimb locomotor performance in the moderately contused adult rat thoracic spinal cord. J Neurosci 2002;22:6670–6681.
24 Kaneko S, Iwanami A, Nakamura M et al. A selective Sema3A inhibitor enhances regenerative responses and functional recovery of the injured spinal cord. Nat Med 2006;12:1380–1389.
25 Okada S, Nakamura M, Katoh H et al. Conditional ablation of Stat3 or Socs3 discloses a dual role for reactive astrocytes after spinal cord injury. Nat Med 2006;12:829–834.
26 Hamzah J, Jugold M, Kiessling F et al. Vascular normalization in Rgs5-deficient tumours promotes immune destruction. Nature 2008; 453:410–414.
27 Longbrake EE, Lai W, Ankeny DP et al. Characterization and modeling of monocyte-derived macrophages after spinal cord injury. J Neurochem 2007;102:1083–1094.
28 Biernaskie J, Sparling JS, Liu J et al. Skin-derived precursors generate myelinating Schwann cells that promote remyelination and functional recovery after contusion spinal cord injury. J Neurosci 2007;27:9545–9559.
29 Simon C, Dondi E, Chaix A et al. Lnk adaptor protein down-regulates specific Kit-induced signaling pathways in primary mast cells. Blood 2008;112:4039–4047.
30 Nobuhisa I, Takizawa M, Takaki S et al. Regulation of hematopoietic development in the aorta-gonad-mesonephros region mediated by Lnk adaptor protein. Mol Cell Biol 2003;23:8486–8494.
31 Fitau J, Boulday G, Coulon F et al. [The adaptor protein Lnk modulates endothelial cell activation]. Nephrol Ther 2005;1:228–233.
32 Fitau J, Boulday G, Coulon F et al. The adaptor molecule Lnk negatively regulates tumor necrosis factor-alpha-dependent VCAM-1 expression in endothelial cells through inhibition of the ERK1 and -2 pathways. J Biol Chem 2006;281:20148–20159.
33 Kwon SM, Suzuki T, Kawamoto A et al. Pivotal role of Lnk adaptor protein in endothelial progenitor cell biology for vascular regeneration. Circ Res 2009;104:969–977.
34 Okumura N, Tsuji K, Ebihara Y et al. Chemotactic and chemokinetic activities of stem cell factor on murine hematopoietic progenitor cells. Blood 1996;87:4100–4108.
35 Lutz M, Rosenberg M, Kiessling F et al. Local injection of stem cell factor (SCF) improves myocardial homing of systemically delivered c-kit+ bone marrow-derived stem cells. Cardiovasc Res 2008;77: 143–150.
36 Asahara T, Chen D, Takahashi T et al. Tie2 receptor ligands, angiopoietin-1 and angiopoietin-2, modulate VEGF-induced postnatal neovascularization. Circ Res 1998;83:233–240.
37 Barrett CP, Donati EJ, Guth L. Differences between adult and neonatal rats in their astroglial response to spinal injury. Exp Neurol 1984; 84:374–385.
38 Bradbury EJ, Moon LD, Popat RJ et al. Chondroitinase ABC promotes functional recovery after spinal cord injury. Nature 2002;416: 636–640.
39 Menet V, Prieto M, Privat A et al. Axonal plasticity and functional recovery after spinal cord injury in mice deficient in both glial fibrillary acidic protein and vimentin genes. Proc Natl Acad Sci U S A 2003; 100:8999–9004.
40 Bush TG, Puvanachandra N, Horner CH et al. Leukocyte infiltration, neuronal degeneration, and neurite outgrowth after ablation of scar-forming, reactive astrocytes in adult transgenic mice. Neuron 1999;23: 297–308.
41 Liberto CM, Albrecht PJ, Herx LM et al. Pro-regenerative properties of cytokine-activated astrocytes. J Neurochem 2004;89: 1092–1100.
42 Shen Q, Wang Y, Kokovay E et al. Adult SVZ stem cells lie in a vascular niche: A quantitative analysis of niche cell–cell interactions. Cell Stem Cell 2008;3:289–300.
43 Tavazoie M, Van der Veken L, Silva-Vargas V et al. A specialized vascular niche for adult neural stem cells. Cell Stem Cell 2008;3: 279–288.
44 Krum JM, Mani N, Rosenstein JM. Angiogenic and astroglial responses to vascular endothelial growth factor administration in adult rat brain. Neuroscience 2002;110:589–604.
45 Zacchigna S, Lambrechts D, Carmeliet P. Neurovascular signalling defects in neurodegeneration. Nat Rev Neurosci 2008;9:169–181.
46 Suri C, Jones PF, Patan S et al. Requisite role of angiopoietin-1, a ligand for the TIE2 receptor, during embryonic angiogenesis. Cell 1996;87:1171–1180.
47 Thurston G, Suri C, Smith K et al. Leakage-resistant blood vessels in mice transgenically overexpressing angiopoietin-1. Science 1999;286: 2511–2514.
48 Thurston G, Rudge JS, Ioffe E et al. Angiopoietin-1 protects the adult vasculature against plasma leakage. Nat Med 2000;6:460–463.
49 Stoeltzing O, Ahmad SA, Liu W et al. Angiopoietin-1 inhibits vascular permeability, angiogenesis, and growth of hepatic colon cancer tumors. Cancer Res 2003;63:3370–3377.
50 Metheny-Barlow LJ, Li LY. The enigmatic role of angiopoietin-1 in tumor angiogenesis. Cell Res 2003;13:309–317.
51 Klapka N, Hermanns S, Straten G et al. Suppression of fibrous scarring in spinal cord injury of rat promotes long-distance regeneration of corticospinal tract axons, rescue of primary motoneurons in somatosensory cortex and significant functional recovery. Eur J Neurosci 2005;22:3047–3058.
52 Stichel CC, Muller HW. The CNS lesion scar: New vistas on an old regeneration barrier. Cell Tissue Res 1998;294:1–9.
53 Dou CL, Levine JM. Inhibition of neurite growth by the NG2 chondroitin sulfate proteoglycan. J Neurosci 1994;14:7616–7628.
54 Bundesen LQ, Scheel TA, Bregman BS et al. Ephrin-B2 and EphB2 regulation of astrocyte-meningeal fibroblast interactions in response to spinal cord lesions in adult rats. J Neurosci 2003;23:7789–7800.
55 Bareyre FM, Kerschensteiner M, Raineteau O et al. The injured spinal cord spontaneously forms a new intraspinal circuit in adult rats. Nat Neurosci 2004;7:269–277.
56 Courtine G, Song B, Roy RR et al. Recovery of supraspinal control of stepping via indirect propriospinal relay connections after spinal cord injury. Nat Med 2008;14:69–74.

See www.StemCells.com for supporting information available online.

Lnk regulates integrin αIIbβ3 outside-in signaling in mouse platelets, leading to stabilization of thrombus development in vivo

Hitoshi Takizawa,[1] Satoshi Nishimura,[2,3,4] Naoya Takayama,[5] Atsushi Oda,[6] Hidekazu Nishikii,[5] Yohei Morita,[5] Sei Kakinuma,[5] Satoshi Yamazaki,[5] Satoshi Okamura,[5] Noriko Tamura,[7] Shinya Goto,[7] Akira Sawaguchi,[8] Ichiro Manabe,[2,3,4] Kiyoshi Takatsu,[9] Hiromitsu Nakauchi,[5] Satoshi Takaki,[1] and Koji Eto[5]

[1]Research Institute, International Medical Center of Japan, Tokyo, Japan. [2]Department of Cardiovascular Medicine, Graduate School of Medicine and [3]Translational Systems Biology and Medicine Initiative, University of Tokyo, Tokyo, Japan. [4]PREST, Japan Science and Technology Agency, Tokyo, Japan. [5]Center for Stem Cell Biology and Regenerative Medicine, Institute of Medical Science, University of Tokyo, Tokyo, Japan. [6]Department of Environmental Medicine, Graduate School of Medicine, Hokkaido University, Sapporo, Japan. [7]Department of Medicine, Tokai University School of Medicine, Isehara, Japan. [8]Department of Anatomy, Faculty of Medicine, University of Miyazaki, Miyazaki, Japan. [9]Preferectural Institute for Pharmaceutical Research, Toyama, Japan.

The nature of the in vivo cellular events underlying thrombus formation mediated by platelet activation remains unclear because of the absence of a modality for analysis. Lymphocyte adaptor protein (Lnk; also known as Sh2b3) is an adaptor protein that inhibits thrombopoietin-mediated signaling, and as a result, megakaryocyte and platelet counts are elevated in *Lnk*$^{-/-}$ mice. Here we describe an unanticipated role for Lnk in stabilizing thrombus formation and clarify the activities of Lnk in platelets transduced through integrin αIIbβ3–mediated outside-in signaling. We equalized platelet counts in wild-type and *Lnk*$^{-/-}$ mice by using genetic depletion of Lnk and BM transplantation. Using $FeCl_3$- or laser-induced injury and in vivo imaging that enabled observation of single platelet behavior and the multiple steps in thrombus formation, we determined that Lnk is an essential contributor to the stabilization of developing thrombi within vessels. *Lnk*$^{-/-}$ platelets exhibited a reduced ability to fully spread on fibrinogen and mediate clot retraction, reduced tyrosine phosphorylation of the β3 integrin subunit, and reduced binding of Fyn to integrin αIIbβ3. These results provide new insight into the mechanism of αIIbβ3-based outside-in signaling, which appears to be coordinated in platelets by Lnk, Fyn, and integrins. Outside-in signaling modulators could represent new therapeutic targets for the prevention of cardiovascular events.

Introduction

Platelet activation is controlled through a series of highly regulated processes and is critical for maintaining normal homeostasis (1). The nature of hemostasis and thrombosis mediated in vivo by activated platelets and its contribution to cardiovascular events remains unclear, however. Particularly challenging has been the characterization of the multicellular network of interactions among platelets, endothelial cells, leukocytes, and erythrocytes that occur during thrombus formation in pathological settings and analysis of the kinetics of platelet activity. Injury to vascular endothelial cells exposes matrix proteins, which induce platelets to adhere to the vessel wall, where they subsequently spread and become activated. At the high shear rates found within the circulation, vWF immobilized on the vessel wall binds to the platelet receptor glycoprotein Ib-V-IX complex (GPIb-V-IX), facilitating platelet adhesion to injured sites, where collagen and/or laminin are exposed (2, 3). Once activated, the adhering platelets secrete soluble mediators to recruit additional circulating platelets, and, through their aggregation, bleeding is stopped. Platelet activation is mediated via several signaling pathways, including the integrin αIIbβ3 pathway (1). Other receptor-ligand interactions, including the binding of GPVI-collagen, $P2Y_1$/$P2Y_{12}$-ADP, and protease-activated G protein–coupled receptor–thrombin (PAR-thrombin), synergistically promote integrin αIIbβ3 activation (inside-out signaling) and the subsequent binding of fibrinogen or vWF to integrin αIIbβ3. This binding triggers signaling that promotes cytoskeletal changes that lead to the spread and stabilization of platelet thrombi through a process termed outside-in signaling (1, 2).

It is also known that αIIbβ3 physically interacts with non–receptor tyrosine kinases such as Src and Syk (4, 5) and that activation of these kinases upon engagement of integrin with fibrinogen contributes to the stability of thrombi in vivo (6). The kinases and adaptors involved in the assembly of the αIIbβ3-based signaling complex are believed to include Syk, lymphocyte cytosolic protein 2 (Lcp2, also known as SH2 domain–containing leukocyte protein of 76 kDa [SLP-76]), Vav, and Fyn-binding protein (Fyb, also known as adhesion and degranulation promoting adaptor protein [ADAP]) (4, 5). Tyrosine phosphorylation of the cytoplasmic domain of the integrin β3 subunit, at least on Tyr747, is required for stable platelet aggregation and the interaction of myosin with the β3 subunit in platelets (7), which is believed to be necessary for full clot retraction (8–10).

Lnk (SH2B adaptor protein 3 [Sh2b3]) belongs to the Src-homology 2 (SH2) adaptor family, which also includes SH2-B (Sh2b1) and adaptor protein with PH and SH2 domains (APS; Sh2b2) (11).

Authorship note: Hitoshi Takizawa and Satoshi Nishimura contributed equally to this work.

Conflict of interest: The authors have declared that no conflict of interest exists.

Citation for this article: *J. Clin. Invest.* doi:10.1172/JCI39503.

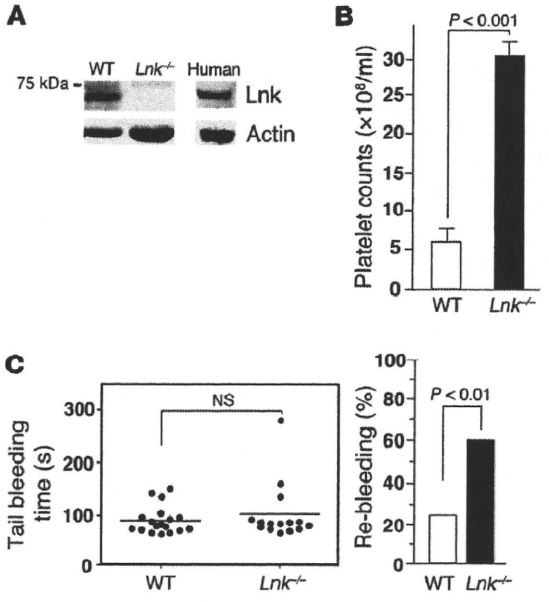

Figure 1
Increased numbers of platelets circulate in *Lnk*$^{-/-}$ mice, but re-bleeding events are increased, while bleeding times are comparable. (**A**) Lnk levels in platelets. Washed platelets from WT and *Lnk*$^{-/-}$ mice or human platelets were lysed and were subjected to immunoblotting with anti-Lnk and anti-actin Abs. (**B**) Platelet counts in EDTA-treated peripheral blood (mean ± SD, $n = 15$ each). (**C**) Tails of WT ($n = 18$) and *Lnk*$^{-/-}$ mice ($n = 15$) were warmed and then transected, immersed in PBS at 37°C, and then monitored for 60 seconds so that any re-bleeding would be detected (detection was positive or negative). Horizontal bars in the left panel show mean in each group.

Lnk-deficient (*Lnk*$^{-/-}$) mouse strains exhibit excessive accumulation of c-Kit$^+$Sca-1$^+$lineage$^-$ (KSL) CD34$^{-/lo}$ HSCs, B cell precursors, erythroblasts, megakaryocytes, and platelets but do not exhibit thrombogenesis and have normal longevity (11–14). The observed phenotypes of *Lnk*$^{-/-}$ mice are caused by a loss of negative regulation by Lnk signaling transduced through several growth factor and cytokine receptors, including the stem cell factor receptor c-Kit, the erythropoietin receptor, and the thrombopoietin receptor c-Mpl (11, 12, 14–17). In the present study, we used an $FeCl_3$-induced injury model and our high-resolution imaging system, which enables observation of single platelet behavior in vivo (18), to examine the function of Lnk in platelets with the aim of clarifying its role in thrombosis. Our results suggest that Lnk promotes stabilization of the developed thrombus, mainly through integrin αIIbβ3-mediated actin cytoskeletal reorganization, and suggest this molecule may represent a new therapeutic target for the treatment and/or prevention of cardiovascular disease.

Results

Thrombus stability is impaired in Lnk$^{-/-}$ *mice in different mouse models of thrombosis.* Lnk is expressed by megakaryocytes, where it acts through integrin signaling to regulate their growth and maturation (14, 19). To determine whether platelets retain Lnk after their release from megakaryocytes and, if so, what its function is, we first used immunoblotting to assess Lnk levels in platelets obtained from WT C57BL/6 mice. This analysis confirmed that substantial amounts of Lnk are retained by WT platelets, and similar results were obtained in humans (Figure 1A). Accordingly, we next investigated the function of Lnk in platelets by examining the effect of Lnk deficiency. As reported previously (14, 19), *Lnk*$^{-/-}$ mice showed a 5-fold increase in platelet number (Figure 1B), though flow cytometry revealed platelet size to be unaffected by the absence of Lnk (data not shown). Moreover, transmission electron microscopic examination revealed that the intracellular structures of resting WT and *Lnk*$^{-/-}$ platelets, including the α- and dense granules, were indistinguishable (Supplemental Figure 1A; supplemental material available online with this article; doi:10.1172/JCI39503DS1). Likewise, the expression levels of the major integrin subunits, αIIb, α2, β3, and β1, as well as GPIbα (the vWF receptor) and GPVI (the collagen receptor), were also similar in WT and *Lnk*$^{-/-}$ platelets (Supplemental Figure 1B).

To examine the functional consequences of Lnk deficiency in mice, we inflicted tail wounds on the mice, after which *Lnk*$^{-/-}$ mice exhibited bleeding times that were comparable to those in WT mice. But whereas 23% of WT mice showed re-bleeding, 60% of *Lnk*$^{-/-}$ mice re-bled ($P < 0.01$ in a χ^2 test, Figure 1C; re-bleeding times did not differ significantly: WT, 58 ± 8 seconds vs. *Lnk*$^{-/-}$, 62 ± 6 seconds), suggesting that thrombi formed in *Lnk*$^{-/-}$ mice are more fragile than those formed in WT mice (1, 8, 20).

To accurately interpret the results summarized above, 2 characteristics of the system had to be taken into account: (a) the numbers of circulating platelets in *Lnk*$^{-/-}$ mice were 5-fold higher than in WT mice (Figure 1B); and (b) Lnk is expressed in endothelial cells as well as platelets (21). In order to exclude the influence of endothelial cells and platelet number, we performed BM transplantation using WT or *Lnk*$^{-/-}$ BM cells. Because it is well established that Lnk deficiency increases stem cell number and enhances the engraftment efficiency upon transplantation (22), we transplanted 1×10^7 BM cells from Ly5.1 WT mice or 2×10^5 or 5×10^5 BM cells from Ly5.1 *Lnk*$^{-/-}$ mice into irradiated 8-week-old Ly5.2 recipient mice, which are hereafter referred to as WT-chimeras and Lnk-chimeras, respectively (Figure 2A). We confirmed that with successful BM replacement (all mice used showed greater than 98% chimerism at Ly5.1/Ly5.2 on myeloid-lineage cells) and with platelets lacking Lnk expression from Lnk-chimeras, the platelet counts in 16-week-old WT-chimeras (8 weeks after transplantation) were comparable to those in 12-week-old Lnk-chimeras (4 weeks after transplantation). By 8 weeks after transplantation, the Lnk-chimeras showed higher platelet counts (Figure 2B). Correspondingly, when compared with WT-chimeras at 8 weeks after transplantation, bleeding times were significantly prolonged in Lnk-chimeras at 4 weeks but not at 8 weeks ($P < 0.01$, Figure 2B). WT-chimeras at 8 weeks, Lnk-chimeras at 4 weeks, and Lnk-chimeras at 8 weeks showed re-bleeding times of 59 seconds (3 of 14 mice), 246 seconds (7 of 14 mice), and 57 seconds (5 of 11 mice), respectively. This suggests that the Lnk deficiency itself contributes to the increased tail bleeding and re-bleeding times. Although there was a high inverse correlation between bleeding times and platelet counts in both

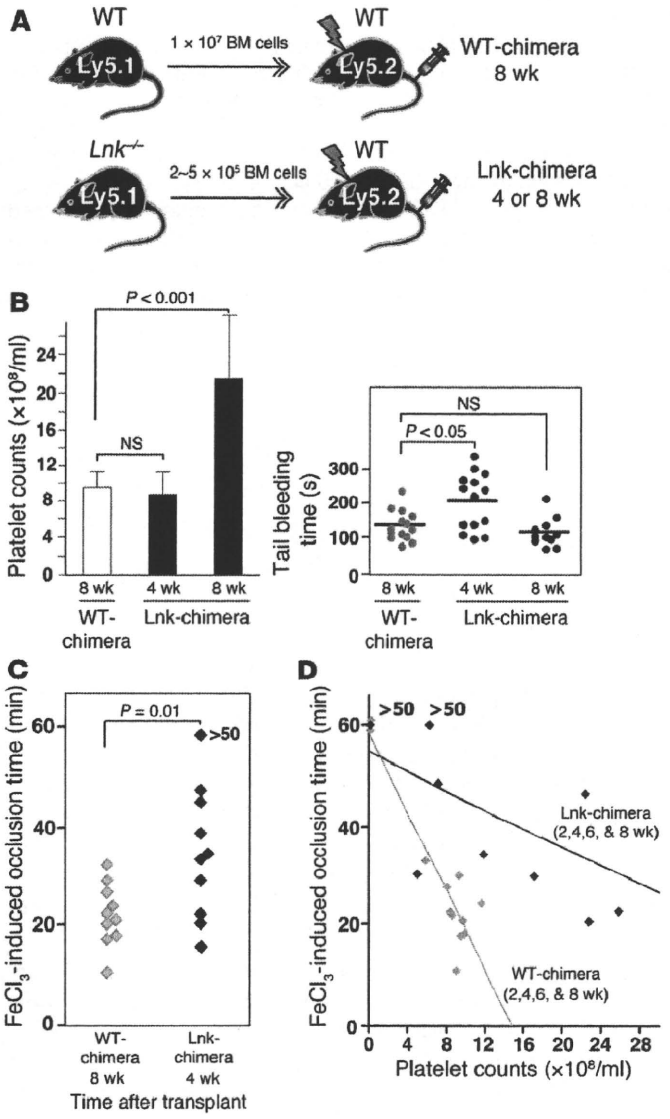

Figure 2

Adjustment of platelet counts through BM transplantation showed prolonged bleeding and occlusion times in a $FeCl_3$-induced thrombosis model. (**A**) The protocol for BM transplantation. (**B**) The left panel shows the platelet counts after transplantation (n = 11–14); data represent mean ± SD. The right panel shows the duration of tail bleeding at the indicated time points; horizontal bars show mean in each group. (**C**) Platelet counts in BM-transplanted mice. WT-chimeras at 8 weeks and Lnk-chimeras at 4 weeks after transplantation were utilized to measure occlusion times during $FeCl_3$-induced thrombosis in carotid arteries (WT-chimera, n = 10; Lnk-chimera, n = 10; P = 0.01). (**D**) Relationship between occlusion times with $FeCl_3$-induced thrombosis and platelet counts in WT- and Lnk-chimeras measured 2, 4, 6, and 8 weeks after transplantation (n = 12 animals in each group). Black symbols denote Lnk-chimeras, while gray ones denote WT-chimeras; the black ($y = -0.96x + 55.0$) and gray lines ($y = -3.94x + 58.6$) are fitted to the data from the Lnk- and WT-chimeras, respectively.

WT- and Lnk-chimeras, irrespective of platelet age or circulating platelet counts (Supplemental Figure 2), the results again suggest that the impaired thrombosis reflects the Lnk deficiency.

We then evaluated occlusion times in carotid arteries exposed to $FeCl_3$ (10% solution on the adventitial side) to induce endothelial injury for assessing thrombus formation in vivo (23). We found that in WT- and Lnk-chimeras with comparable platelet counts, occlusion times were significantly longer in the Lnk-chimeras, which is also indicative of a functional defect in *Lnk*$^{-/-}$ platelets (WT-chimera, n = 10; Lnk-chimera, n = 10; P = 0.01, Figure 2C). When we analyzed for the relationship between occlusion times and platelet counts in the chimeras 2, 4, 6, and 8 weeks after transplantation, there was a high inverse correlation between occlusion times and platelet counts. Of note, however, Lnk-chimeras exhibited longer occlusion times than WT-chimeras with similar platelet counts (Figure 2D), further confirming that Lnk deficiency impairs thrombus formation.

To assess the functionality of *Lnk*$^{-/-}$ platelets in more detail, we used a direct visual technique that enabled us to evaluate in vivo thrombus stability with much greater temporal and spatial resolution and to characterize the kinetics of *Lnk*$^{-/-}$ platelet activity involved in thrombus formation. This method is based on confocal laser microscopy and permits high spatiotemporal resolution of individual platelets under flow conditions in mesenteric capillaries and arterioles (24). With this system, laser irradiation produces ROS, which cause injury to the endothelial layer of the vessels (18). Because laser-induced thrombosis reportedly differs from the $FeCl_3$-induced injury model in terms of the mechanism of thrombus formation (25, 26), we again used WT-chimeras 8 weeks after transplantation and Lnk-chimeras 4 weeks after transplantation, as we did in the experiments shown in Figure 2C. We found that WT- and Lnk-chimeras showed similar single platelet kinetics in the absence of injury, including transient interactions with the endothelium (data not shown). After laser-induced injury, however, thrombus formation was severely diminished in the Lnk-chimeras.

After laser-induced injury to mesenteric capillaries, platelets adhered to the vessel walls at similar rates in the WT- and Lnk-chimeras (WT-chimeras, 1.59 ± 0.18 platelets/ms/μm vs. Lnk-chimeras, 1.48 ± 0.19 platelets/ms/μm; n = 30 vessels from 5 animals, P = 0.44). In the WT-chimeras, the adherent platelets caused platelets in the flowing blood to acutely pile up, and the resultant thrombus reduced the vessel lumen diameter and blood flow velocity. Ultimately, the blood vessel was completely occluded by plugged erythrocytes and/or leukocytes. By contrast, in the Lnk-chimeras, platelets adhered to the vessel wall more loosely than in WT-chimeras, so that they were frequently washed away by the blood flow. As a consequence, the number of platelets that piled up and the size of the resultant thrombus were smaller than in WT-chimeras (Figure 3A and Supplemental Videos 1 and 2). More intriguingly, in both Lnk- and WT-chimeras 2, 4, 6, and 8 weeks after transplantation, the number of platelets adhering to the vessel walls during thrombus formation appeared to be well correlated with the circulating platelet count. However, when we compared thrombus formation in Lnk- and WT-chimeras with similar platelet counts, there was a tendency for animals with *Lnk*$^{-/-}$ platelets (Lnk-chimeras) to show impaired thrombus formation, as compared with WT-chimeras. Moreover, the greatly increased platelet numbers in *Lnk*$^{-/-}$ animals did not enhance thrombus formation to levels similar to those seen in WT-chimeras (Figure 3B), which suggests that Lnk deficiency is itself a factor that contributes to the impaired stabilization of developing thrombi in our laser-induced injury model.

We also applied the laser-induced injury model to compare thrombosis in mesenteric capillaries and arterioles of 12-week-old

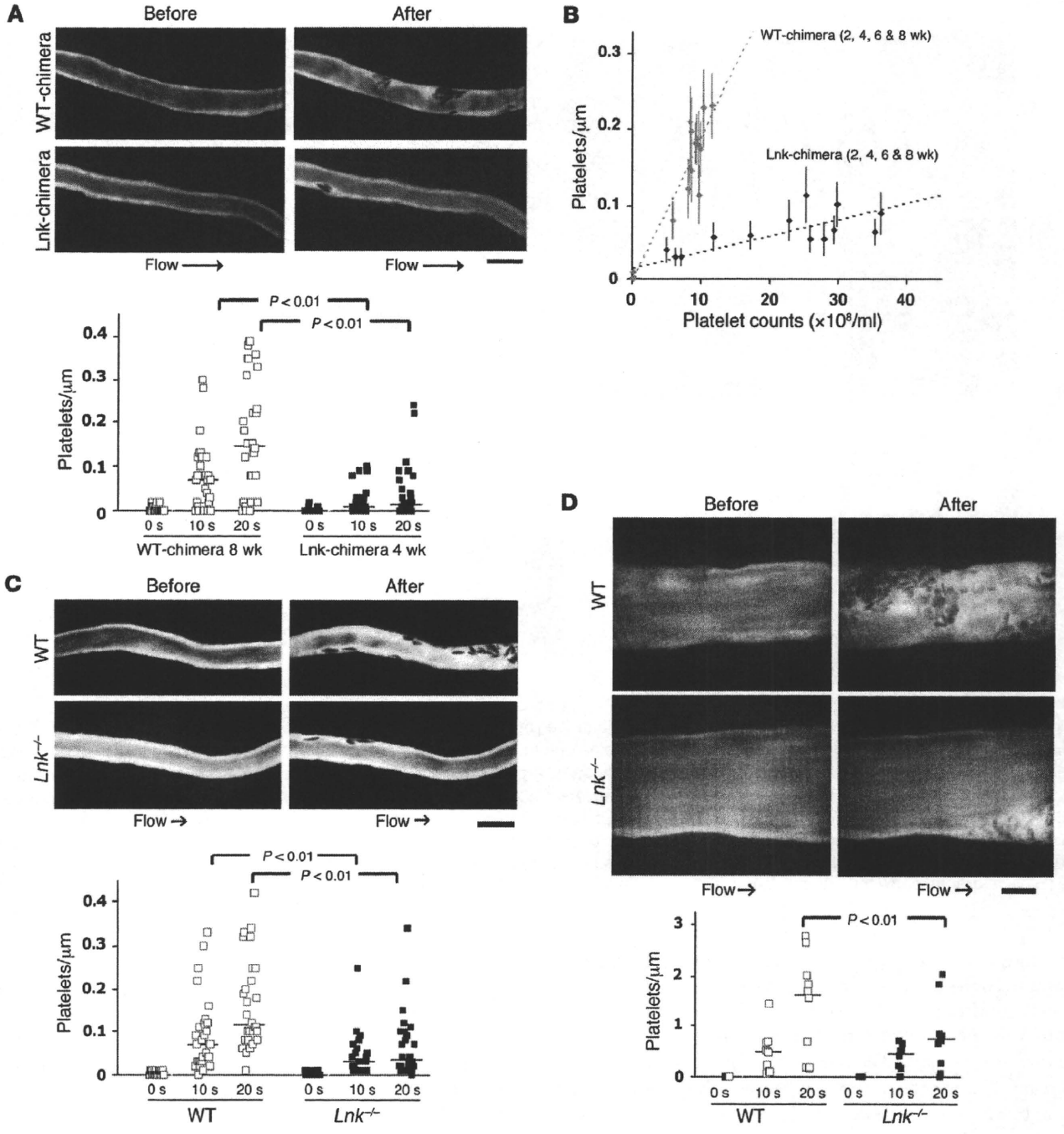

Figure 3

In vivo thrombus formation was impaired in Lnk-chimeras and *Lnk*$^{-/-}$ mice in a laser-induced injury model. (**A**, **C**, and **D**) Video stills of mesenteric capillaries (**A** and **C**) and arterioles (**D**) obtained using intravital fluorescence microscopy before and 20 seconds after laser-induced injury. The numbers of platelets in developing thrombi after laser injury to capillaries (**A** and **C**, lower panel) and arterioles (**D**, lower panel) were calculated. In **A**, **C**, and **D**, *y* axes represent the numbers of platelets per micrometer of observed vessel length. In **A**, results from WT-chimeras 8 weeks after transplantation (16 weeks old) and Lnk-chimeras 4 weeks after transplantation (12 weeks old) are shown ($n = 5$ each). (**B**) Relationship between platelet counts and laser-induced thrombosis. All recipient mice were studied 2, 4, 6, or 8 weeks after transplantation ($n = 17$ animals for each groups). For each mouse, the numbers of platelets per micrometer contributing to thrombi after 20-second injuries to 10 mesenteric capillaries are shown as mean ± SEM along with platelet count. Black and gray dotted lines are fitted to the data from the Lnk- and WT-chimeras, respectively. (**C** and **D**) Results from 12-week-old WT and *Lnk*$^{-/-}$ mice ($n = 5$ each). See Supplemental Videos 1–6 for original movies. Note the impaired thrombus formation in *Lnk*$^{-/-}$ mice in both capillaries and arterioles. Scale bars: 10 μm. Horizontal lines indicate the median values in **A**, **C**, and **D**.

WT and *Lnk*$^{-/-}$ mice (Figure 3, C and D, for capillaries and arterioles, respectively). Upon laser-induced injury, the platelet kinetics in *Lnk*$^{-/-}$ mice were similar to those seen in the Lnk-chimeric mice 4 weeks after transplantation. Initial attachment of the platelets to the vessel wall was observed; however, stable thrombus formation, including the piling up of platelets, was diminished in manner similar to that seen in the Lnk-chimeras. As a result, the numbers of platelets making up the thrombi were significantly reduced in

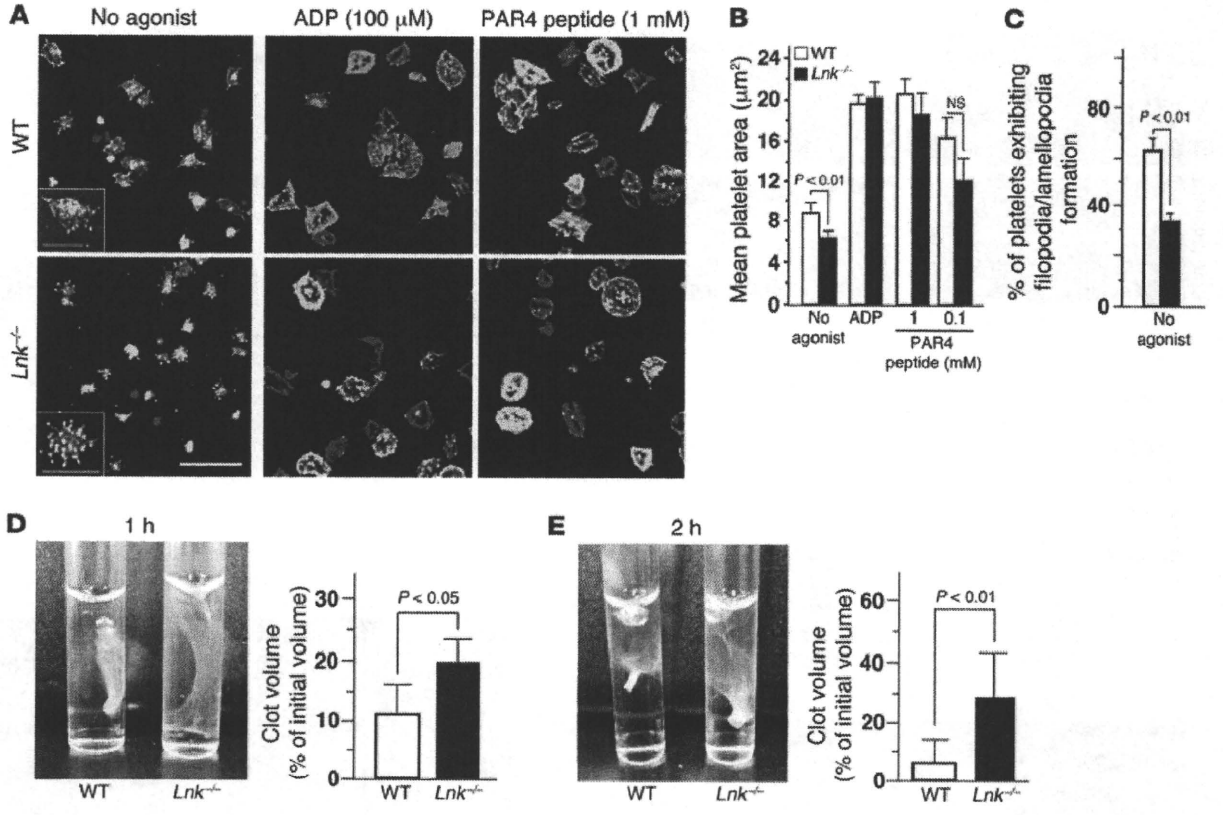

Figure 4

Lnk$^{-/-}$ platelets show defective αIIbβ3-dependent spreading on fibrinogen and fibrin clot retraction. (**A**) Washed platelets from WT and *Lnk*$^{-/-}$ mice were plated on fibrinogen-coated coverslips for 45 minutes. In some preparations, 100 μM ADP or 0.1 or 1 mM PAR4 receptor–activating peptide was present. Cells were fixed, permeabilized, and stained with rhodamine-phalloidin to visualize F-actin (red) and with anti-phosphotyrosine mAb (green). Scale bars: 10 μm (white); 4 μm (insets, orange). (**B**) Platelet spreading was quantified by computer analysis of their surface areas. Each bar in **B** represents the value (mean ± SD) from at least 250 platelets. (**C**) Percentages of platelets exhibiting filopodia or lamellipodia. Twenty sections (20–30 cells/section) were analyzed, and mean ± SD is shown. (**D** and **E**) Fibrin clot retraction was assessed at 1 and 2 hours after addition of thrombin, fibrinogen, and $CaCl_2$ to washed platelets from WT or *Lnk*$^{-/-}$ mice. The images show representative results at 1 (**D**) and 2 hours (**E**). The graphs show the summarized results at 1 (**D**) and 2 hours (**E**) (mean ± SD, $n = 10$ each).

both mesenteric capillaries (Figure 3C and Supplemental Videos 3 and 4) and arterioles (Figure 3D and Supplemental Videos 5 and 6). Taken together, the results indicate that the observed phenotype for thrombus formation caused by the Lnk deficiency is attributable to platelet function, per se, and does not reflect changes in endothelial cell function. This is noteworthy, as it suggests that there could be less thrombus formation in the Lnk-chimeras than in *Lnk*$^{-/-}$ mice, as the higher platelet counts in the latter might slightly compensate for their diminished functionality (Figure 3, A–C).

Lnk promotes integrin αIIbβ3-mediated actin cytoskeletal reorganization but not agonist-dependent integrin activation. To determine the basis for the instability of thrombi formed by *Lnk*$^{-/-}$ platelets, we examined their ability to adhere to fibrinogen-coated plates and their morphology after spreading, both of which are dependent on outside-in αIIbβ3 signaling (1, 8, 27). The initial adhesion of *Lnk*$^{-/-}$ platelets to fibrinogen-coated plates in the absence of agonistic stimuli appeared normal, as did formation of filopodial projections (data not shown). On the other hand, their subsequent spreading (after 15 minutes) was impaired, and formation of a lamellipodial edge was incomplete (shown at 45 minutes, Figure 4A, "No agonist") (28, 29). The mean area covered by the adhering platelets and the percentage of platelets showing filopodia and/or lamellipodia (percentage of spreading) were both significantly reduced in the absence of Lnk (at 45 minutes, Figure 4, B and C; time-dependent change in mean area without agonist, Supplemental Figure 3A). This suboptimal spreading of *Lnk*$^{-/-}$ platelets was not observed when they were stimulated with a high concentration of a G protein–coupled receptor agonist such as 100 μM ADP or 1 mM PAR4-activating peptide (sequence: AYPGKF) (Figure 4, A and B), although lower concentrations of agonists, such as 0.1 mM PAR4-activating peptide (Figure 4B) or 0.05 U/ml thrombin (Supplemental Figure 3B), did not completely restore the spreading on immobilized fibrinogen impaired by Lnk deficiency, even when the secretion of effectors from platelet granules was blocked (Supplemental Figure 3B). In addition, there was no significant difference in the reduction in the spread areas of platelets from Lnk-chimeras 4 weeks and 8 weeks after transplantation (data not shown), indicating that the impaired spreading caused by Lnk deficiency is independent of platelet age after myelosuppression. Thus, Lnk appears to continuously participate in a subset of αIIbβ3- and actin-dependent morphological responses triggered by platelet adhesion to fibrinogen (1) independently of its negative impact on proliferation in HSCs and megakaryocytes (12, 14, 19).

Another platelet response that is dependent on αIIbβ3 and the actin cytoskeleton is fibrin clot retraction (8, 9, 27), which we examined using equal numbers of *Lnk*$^{-/-}$ and WT washed platelets

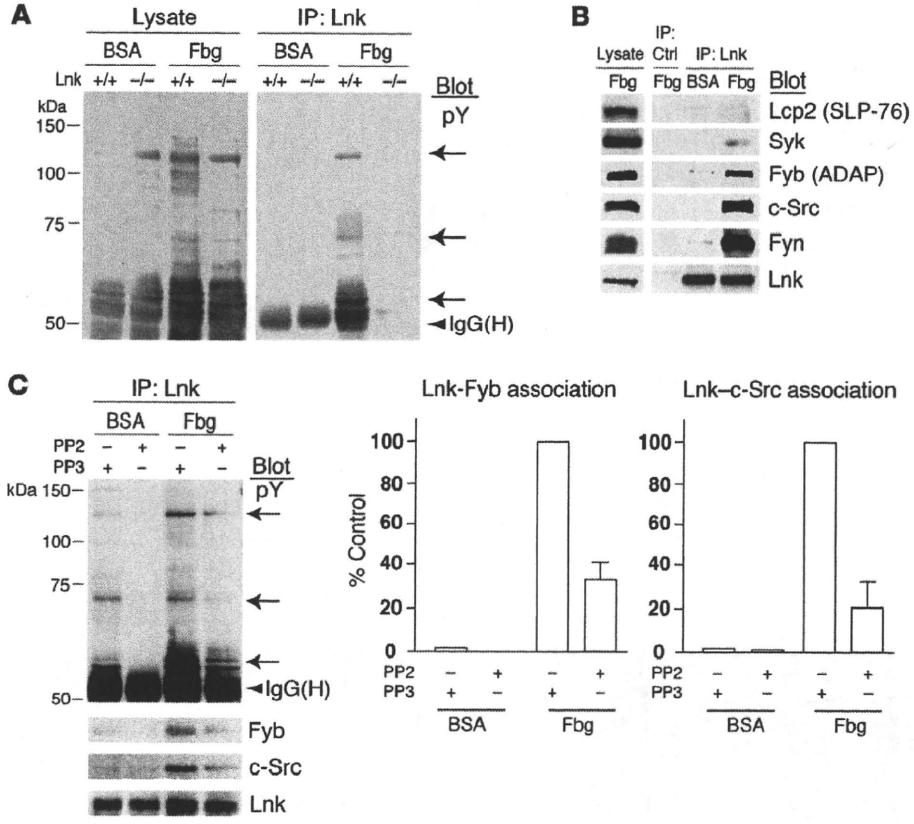

Figure 5

Lnk associates with c-Src, Fyn, and Fyb in a manner dependent on outside-in signaling. (**A**) Washed platelets from WT and *Lnk*$^{-/-}$ mice were plated on fibrinogen (Fbg) for 45 minutes or maintained in suspension in a BSA-coated dish. Platelet lysate (left) or proteins immunoprecipitated using anti-Lnk Abs (right, IP: Lnk) were separated and probed with anti-phosphotyrosine (pY) mAb. (**B**) Lysates from WT platelets prepared as in **A** and immunoprecipitates obtained using irrelevant control rabbit sera (IP: Ctrl) or anti-Lnk (IP: Lnk) were probed by immunoblotting for the indicated proteins. (**C**) WT platelets were incubated with 5 μM PP2 to block Src kinase activity or with PP3, an inactive congener of PP2. PP2 but not PP3 diminished tyrosine phosphorylation of cellular proteins and the association of c-Src and Fyb, with Lnk in platelets adhering to fibrinogen. The observation was confirmed using 20 μM SU6656, an unrelated selective c-Src inhibitor (data not shown). Arrows indicate bands for the expected phosphoproteins corresponding to Fyb, Lnk, and c-Src. Results shown are representative of 3 independent experiments. The 2 panels on the right show the quantification of Western blot bands from 3 experiments (mean ± SD). Maximal band density was defined as 100%.

in the presence of fibrinogen, $CaCl_2$, and thrombin (Figure 4, D and E). Under these conditions, the clot retraction seen with *Lnk*$^{-/-}$ platelets was slower and less effective than that seen with WT platelets, which is consistent with the idea that platelet responses are dependent on αIIbβ3-mediated actin cytoskeletal signaling and that Lnk is involved. To further study the role of αIIbβ3 activation in *Lnk*$^{-/-}$ platelets, we also used flow cytometry to quantify the specific binding of Alexa Fluor 488–conjugated fibrinogen to washed platelets upon stimulation with various concentrations of ADP, epinephrine, PAR4 peptide, phorbol myristate acetate, or convulxin (CVX), which selectively stimulates GPVI (Supplemental Figure 4A). We found that *Lnk*$^{-/-}$ and WT platelets showed similar fibrinogen binding, irrespective of the agonist inducing the inside-out signaling. In addition, levels of P-selectin expression were indistinguishable (Supplemental Figure 4B), suggesting that Lnk is not involved in α-granule secretion.

Lnk recruitment to the αIIbβ3-based signaling complex is dependent on outside-in signaling and c-Src activation. To understand the mechanism by which Lnk regulates outside-in signaling, we sought the molecule(s) that associates with Lnk in platelets. One prominent cellular event required for integrin-dependent responses is tyrosine phosphorylation of several cytosolic proteins (Figure 5A) (1, 4, 27). Incubation of WT platelets on fibrinogen induced tyrosine phosphorylation of cellular proteins with molecular weights of 60, 65–75, 90–110, and 120–130 kDa, but much less post-engagement tyrosine-phosphorylation was seen in *Lnk*$^{-/-}$ platelets. In addition, immunoprecipitation assays revealed that several phosphoproteins associate with Lnk (the 68-kDa protein was likely Lnk itself). A variety of proteins, including Syk, LCP2, and Fyb, are known to be tyrosine phosphorylated in an Src-dependent manner in fibrinogen-adherent platelets (29, 30). In the present study, both c-Src and Fyb co-immunoprecipitated with Lnk from WT platelets adhering to fibrinogen but not from unstimulated ones; Syk was only weakly detectable, and LCP2 was barely so (Figure 5B). It has also been proposed that Fyn, an Src-family protein, may contribute to integrin αIIbβ3 signaling (9, 20), and we found that, like c-Src, Fyn associated with Lnk in stimulated platelets (Figure 5B).

c-Src and Fyn are known to associate with the cytoplasmic tail of the integrin β3 subunit in vitro (20, 31), which suggests that after platelets bind to fibrinogen, Lnk regulates the assembly of an αIIbβ3-based signaling complex (5). We therefore asked whether the observed association of c-Src and/or Fyb with Lnk is dependent on Src kinase activity. When platelets were incubated with 5 μM PP2 (to block Src kinase activity) or PP3 (an inactive congener of PP2), PP2 but not PP3 diminished tyrosine phosphorylation of cellular proteins and the association of c-Src and Fyb with Lnk in platelets adhering to fibrinogen (Figure 5C). To then confirm that the phosphorylation of Lnk and its association with c-Src are dependent on c-Src activation, we used a COS7 cell expression system to evaluate the interaction in more detail (Supplemental Figure 5A). Flag-tagged WT Lnk (WT-Lnk) or a mutant form lacking the C-terminal portion containing Tyr536 (ΔC-Lnk) was expressed in COS7 cells in the presence and absence of a constitutively active form of human c-Src (Y530F, CA-Src). Whereas WT-Lnk became tyrosine phosphorylated when coexpressed with CA-Src, ΔC-Lnk showed little or no phosphorylation, indicating that Tyr536 is a key target site for phosphorylation by c-Src (Supplemental Figure 5A). On the other hand, a constitutively active form of Fyn did not phosphorylate WT-Lnk (data not shown). We then evaluated the consequences of the loss of c-Src–mediated Lnk phosphorylation using CHO cells, which constitutively express human αIIbβ3 (29, 32) and were previously shown to spread on immobilized fibrino-

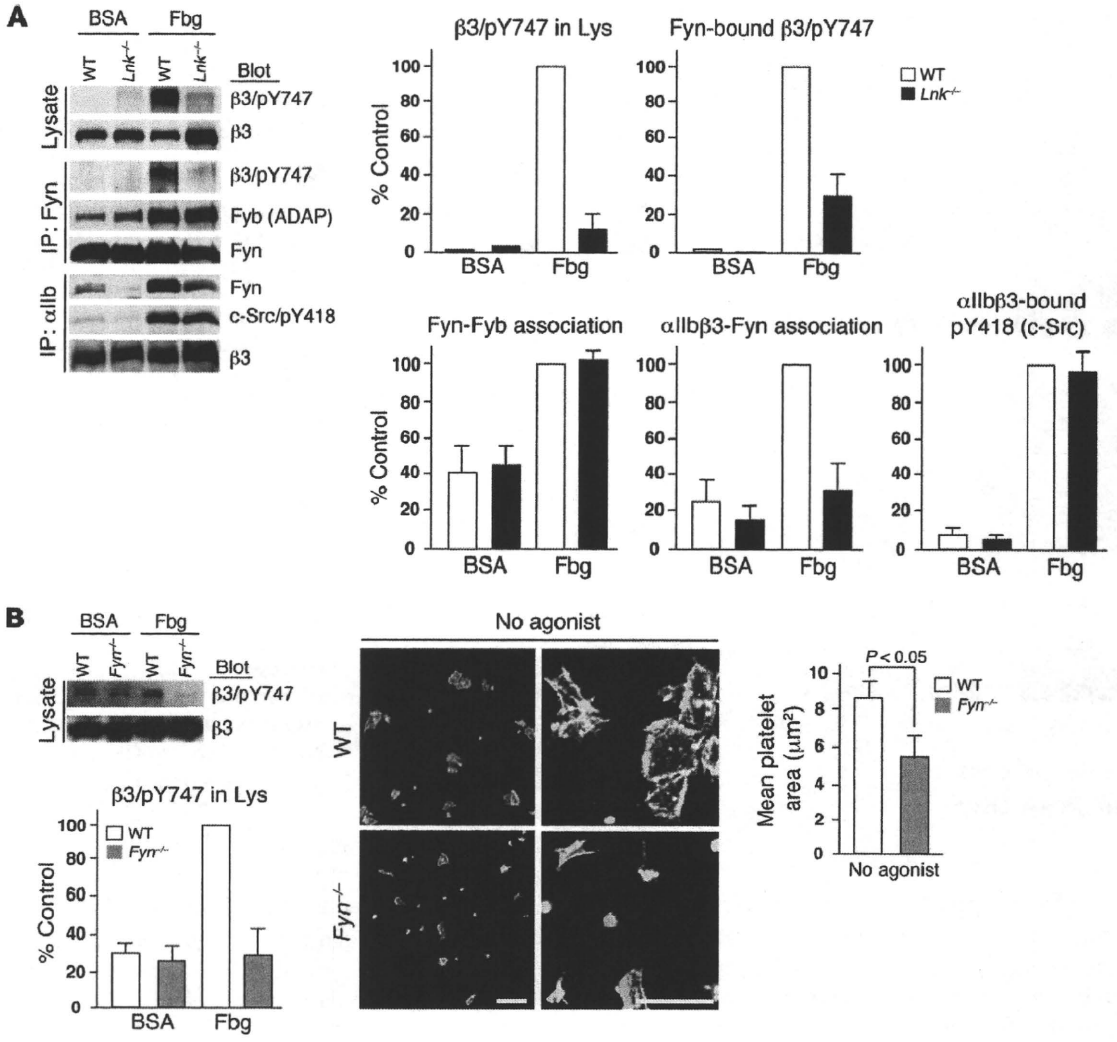

Figure 6

Lnk deficiency in platelets leads to reduced binding of Fyn to αIIbβ3 and reduced tyrosine phosphorylation of the cytoplasmic domain of the β3 integrin subunit. (**A**) WT and *Lnk*$^{-/-}$ platelets plated or maintained in suspension as in Figure 5A were lysed and analyzed by immunoblotting using anti–β3 integrin or anti–β3/p-Tyr747. In other sets, immunoprecipitation was elicited with anti-Fyn or anti-αIIb Ab. Each immunoblot panel is representative of 3 or 4 independent experiments, and estimated band densities are shown in the graphs. Band densities for WT samples from adherent platelets on fibrinogen were defined as 100%. Lys, lysates. (**B**) Washed platelets from WT and *Fyn*$^{-/-}$ mice were plated on fibrinogen for 45 minutes or maintained in suspension in a BSA-coated dish, lysed, and analyzed. The error bars in **A** and **B** indicate mean ± SD. (**C**) Left panels show the features of WT or *Fyn*$^{-/-}$ platelets allowed to spread on fibrinogen-coated coverslips for 45 minutes in the absence of agonist. The cells were fixed, permeabilized, and stained with Alexa 488 Fluor–phalloidin to visualize F-actin. Scale bars: 10 μm. The graph shows spreading quantified by computer analysis of their surface areas (mean ± SD).

gen in an Src kinase–dependent manner (32). When WT-Lnk or ΔC-Lnk was expressed as a GFP fusion protein, CHO cells expressing ΔC-Lnk showed fewer lamellipodia on fibrinogen than those expressing WT-Lnk (Supplemental Figure 5B). Thus, the absence of its C terminus again disrupted Lnk's ability to mediate formation of lamellipodia (Supplemental Figure 5B). Apparently, the C-terminal portion of Lnk and phosphorylation of Tyr536, which is likely regulated by c-Src, are key contributors to formation of lamellipodia and cell spreading mediated via integrin αIIbβ3.

Adherent Lnk$^{-/-}$ *platelets show reduced tyrosine phosphorylation of the β3 integrin subunit and reduced association of Fyn with αIIbβ3.* The importance of Src activation to outside-in αIIbβ3 signaling is well documented (4, 5, 31). Because Lnk appears to co-immunoprecipitate with both c-Src and Fyn (Figure 5B), we next asked whether Lnk might regulate the function of these kinases in platelets. During platelet aggregation or adhesion to fibrinogen, 2 conserved tyrosine residues in the β3 subunit, Tyr747 and Tyr759, are putatively targeted by Fyn, which is reportedly indispensable for clot retraction and prevention of re-bleeding from tail wounds (1, 8, 9). Moreover, Tyr747 is reportedly required for the binding of talin, filamin, c-Src, and other proteins essential for normal integrin signaling in platelets (33). We previously observed prominent phosphorylation of Tyr747 in WT platelets upon adherence to fibrinogen (10), but this response was severely impaired in *Lnk*$^{-/-}$ platelets (Figure 6A). Because it is likely that Fyn phosphorylates Tyr747 through direct interaction with the β3 cytoplasmic tail (9, 20, 31), we examined the extent to which Lnk deficiency affected (a) the association of Fyn with β3 and (b) the phosphorylation status of Tyr747 in plate-

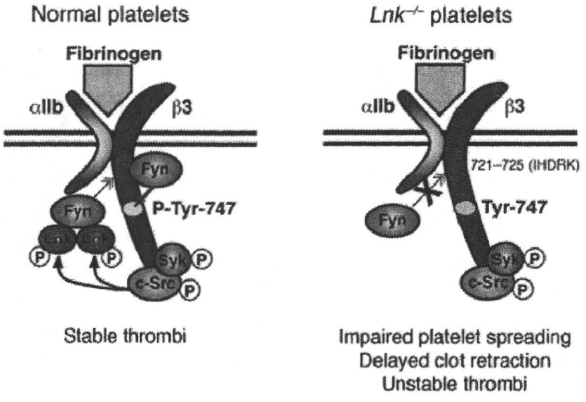

Figure 7

Model for outside-in signaling through αIIbβ3, c-Src, Fyn, and Lnk. Based on the present study, we propose that when activated, αIIbβ3 binds to fibrinogen, and a pool of c-Src constitutively bound to the cytoplasmic domain of the integrin β3 subunit initiates outside-in αIIbβ3 integrin signaling, which includes phosphorylation of Syk and its recruitment to αIIbβ3 independent of Lnk (5). The activated c-Src phosphorylates Tyr536 in a C-terminal portion of Lnk, where Lnk forms a dimeric or multimeric structure via the N-terminal domain (34). Lnk strongly facilitates Fyn recruitment to its binding site, residues 721–725 (IHDRK) in the β3 integrin tail, which may lead to phosphorylation of Tyr747 (P-Tyr747) within the β3 cytoplasmic domain of integrin αIIbβ3. Thereafter, phosphorylation of Tyr747 may facilitate thrombus stabilization in vitro and in vivo through a platelet contraction mechanism (7, 9, 40).

lets. We found that in WT platelets, Fyn co-immunoprecipitated with phosphorylated β3 and that this response was dependent upon fibrinogen ligation (Figure 6A, IP: Fyn). Furthermore, Fyn was bound to αIIbβ3 complexes immunoprecipitated 0 and 45 minutes after fibrinogen binding (Figure 6A, IP: αIIb, lanes BSA and Fbg, respectively), but this interaction was markedly diminished in *Lnk*$^{-/-}$ platelets at the same time point. The association of Fyn with Fyb was augmented by fibrinogen binding independently of Lnk (Figure 6A, IP: Fyn), and the activation of c-Src bound to αIIbβ3 (assessed based on phosphorylation of Tyr418) was comparable (Figure 6A, IP: αIIb). That Fyn is constitutively associated with the β3 integrin subunit (20) suggests that Lnk contributes to the maintenance or strength of Fyn binding to the αIIbβ3-based signaling complex without affecting c-Src activation.

Finally, we assessed the effect of Fyn deficiency on tyrosine phosphorylation of the β3 subunit and the morphology of platelets spread on fibrinogen. *Fyn*$^{-/-}$ platelets showed reduced phosphorylation of at least Tyr747 when bound to fibrinogen for 15 or 45 minutes (shown at 45 minutes, Figure 6B). In addition, in the absence of an agonist, *Fyn*$^{-/-}$ platelets exhibited delayed and impaired spreading and somewhat reduced formation of lamellipodia on fibrinogen, even after 45 minutes (Figure 6C). *Fyn*$^{-/-}$ platelets began spreading at about 20 minutes, by which time the spreading of WT platelets had already reached a plateau (data not shown). These results are consistent with the idea that Lnk sustains Fyn kinase activation of αIIbβ3, thereby regulating tyrosine phosphorylation of the β3 subunit.

Fyn-deficient mice exhibit a defect in thrombus formation similar to that seen in Lnk-deficient mice. To further examine the role of Fyn during thrombus formation in vivo, we assessed thrombus formation within mesenteric capillaries and arteries as we did for Lnk in the experiments shown in Figure 3, C and D. We found that *Fyn*$^{-/-}$ mice exhibited impaired thrombus formation that was very similar to that seen in *Lnk*$^{-/-}$ mice (Supplemental Figure 6 and Supplemental Videos 7 and 8). They also showed increased re-bleeding, but not prolonged initial bleeding times (data not shown), which is consistent with the results of Reddy et al. (20). Thus, Lnk and Fyn may act in concert to regulate αIIbβ3-based actin cytoskeletal reorganization leading to thrombus stabilization.

Discussion

Lnk is known to be a negative modulator of cytokine/growth factor receptor–mediated signaling (22) and to, perhaps, influence the motility of HSCs and progenitor cells, including their homing to (or lodging within) niches within the BM (16, 34). In addition, the proven importance of integrins and actin reorganization in HSC migration and homing (34, 35) and in megakaryocyte function (19) raises the possibility that Lnk modulates integrin signaling, but this idea has yet to be tested. In this report, we revealed a formerly unrecognized mechanism by which Lnk adaptor protein regulates integrin signaling in platelets and stabilizes developing thrombi in vivo. Using an in vivo $FeCl_3$-induced vessel occlusion model and direct imaging of platelet behavior, we showed that Lnk deficiency in platelets impairs stabilization of the developing thrombus under flow conditions, which may lead to an increase in re-bleeding events in *Lnk*$^{-/-}$ (Figure 1C) and Lnk-chimeric (Supplemental Figure 2, right) mice. Through these mechanistic studies, we have been able to demonstrate that Lnk is required for platelets to fully spread on fibrinogen (Figure 4 and Supplemental Figure 3), for efficient fibrin clot retraction (Figure 4C), for platelet aggregation in the presence of lower concentrations of an agonist (Figure 4D), and for thrombus stability under flow conditions in vivo (Figures 2 and 3). Furthermore, the findings show that all of these effects of Lnk are mediated largely by αIIbβ3-dependent outside-in signaling, which is likely associated with tyrosine phosphorylation of the β3 integrin subunit (8) or Fyn tyrosine kinase (20). We also found that ligand binding to αIIbβ3 in platelets induces the formation of a protein complex that includes αIIbβ3, c-Src, Fyn, Fyb, and Lnk (Figure 5). Formation of this complex required Src kinase activity, which targeted the C-terminal portion of Lnk (Supplemental Figure 5). Finally, we showed that Lnk supports activation of Fyn within the αIIbβ3 complex, that Fyn in turn tyrosine phosphorylates the β3 subunit (Figure 6), and that the consequences of Lnk deficiency are mirrored by Fyn deficiency (Supplemental Figure 6). In contrast to the previously described constitutive association of c-Src or Fyn with β3 (4, 31), our results indicate that the efficient binding of Fyn, but not c-Src, to the αIIbβ3 complex requires the presence of Lnk (Figure 6). When situated in close proximity to αIIbβ3, Fyn may function as a positive regulator of β3 tyrosine phosphorylation (Figure 6B) (10, 28), which would contribute to the stabilization of the thrombus (Supplemental Figure 6) (9, 20), perhaps through association of Fyn with EphA4 (7) or Bcl-3 (36). Lnk thus appears to play a previously unappreciated role in facilitating integrin αIIbβ3 outside-in signaling by acting in concert with Fyn to phosphorylate the β3 subunit on Tyr747, thereby optimizing platelet cytoskeletal reorganization for stabilization of thrombi in vivo. We therefore conclude that Lnk may selectively promote Fyn kinase regulation of αIIbβ3 outside-in signaling in platelets.

One limitation of comparing thrombus formation in Lnk- and WT-chimeras is the need to compare platelets in mice of differ-